TN 2440

NACA TN 2440

RECEIVED
28 AUG 1951
BAGR-WD
LOS ANGELES

NATIONAL ADVISORY COMMITTEE FOR AERONAUTICS

TECHNICAL NOTE 2440

WIND-TUNNEL INVESTIGATION AND ANALYSIS OF THE EFFECTS OF END PLATES ON THE AERODYNAMIC CHARACTERISTICS OF AN UNSWEPT WING

By Donald R. Riley

Langley Aeronautical Laboratory
Langley Field, Va.

Washington
August 1951

TECHNICAL LIBRARY
AIRESEARCH MANUFACTURING CO.
9851-9951 SEPULVEDA BLVD.
LOS ANGELES 45,
CALIFORNIA

NATIONAL ADVISORY COMMITTEE FOR AERONAUTICS

TECHNICAL NOTE 2440

WIND-TUNNEL INVESTIGATION AND ANALYSIS OF THE EFFECTS OF END PLATES ON THE AERODYNAMIC CHARACTERISTICS OF AN UNSWEPT WING

By Donald R. Riley

SUMMARY

A wind-tunnel investigation has been conducted to determine the effects of end plates of various areas and shapes on the aerodynamic characteristics of an unswept and untapered wing of aspect ratio 4.

The results were in agreement with those of previous investigations in that the end plates provided the basic wing with an increase in the lift-curve slope, a reduction in the induced drag, and an increase in the maximum lift coefficient. Negligible variations were obtained in the pitching moment when the end plates were added. A reduction of the experimental data, in which the end-plate effect was expressed in terms of an effective aspect ratio, was in fair agreement with the classical theory for evaluating the end-plate effects on the lift-curve slope and induced drag.

Expressions for the lift-drag and maximum lift-drag ratios, developed herein for the wing-end-plate configuration, gave predictions that compared favorably with experimental values. A theoretical analysis of these two expressions indicates that the use of end plates may provide relatively large increases in the lift-drag ratio at the higher lift coefficients for a limited range of end-plate areas but that end plates cannot be expected to provide substantial increases in the maximum lift-drag ratio of the wing. The most favorable effect of end plates on the maximum lift-drag ratio of a wing is obtained when the wing aspect ratio is low and the ratio of wing profile drag coefficient to end-plate profile drag coefficient is high. For such cases, however, the absolute value of the maximum lift-drag ratio is, of necessity, rather low.

In the case of wing-body combinations or complete airplanes, for which the total drag of components other than the wing may be large relative to the wing drag, substantial increases in maximum lift-drag ratio apparently may be obtained by the use of appropriately designed

end plates. The increase obtained with end plates, except possibly for small end plates, is not likely to be as large, however, as that which would be obtained by utilizing the end-plate area as a simple addition to the wing tips to increase the wing span and hence the wing geometric aspect ratio. The use of end plates as a means of improving the lift-drag ratios of airplanes, therefore, would seem to be of primary importance when it is desired to keep the wing span as small as possible.

INTRODUCTION

The use of end plates as a possible means of improving the aerodynamic characteristics of unswept wings has been investigated in references 1 to 5. The results of these investigations indicate that the end plates provide an increase in the lift-curve slope, a reduction in the induced drag, and an increase in the maximum lift coefficient of the basic wing. Heretofore, theoretical and empirical analyses on end-plate effects have been concerned mainly with predicting the lift-curve slope and the induced drag and, as a result, have yielded relatively few conclusions on the effect of end plates on the lift-drag and maximum lift-drag ratios. The favorable effects of end plates on the lift and induced drag have suggested the possibility of using end plates as a means of increasing the lift-drag and maximum lift-drag ratios of the basic wing. The effect of end plates on sweptback wings has also been investigated and the results are presented in reference 6.

The present investigation was conducted in the Langley stability tunnel to determine the effects of end plates of various areas and shapes on the aerodynamic characteristics of an unswept and untapered wing of aspect ratio 4. The results serve the purpose of checking the validity of current methods of predicting the end-plate effect on the lift-curve slope and the induced drag. In addition, expressions are developed herein for the lift-drag and maximum lift-drag ratios and the calculated results are compared with values obtained from the experimental data. A theoretical analysis of the lift-drag and maximum lift-drag ratios is presented in order to indicate the influence of the various factors affecting these two aerodynamic characteristics.

SYMBOLS

The data presented herein are in the form of standard NACA coefficients of forces and moments which are referred to the system of wind axes with the origin coinciding with the intersection of the wing quarter-chord line and the plane of symmetry. The coefficients and symbols are defined as follows:

L	lift, pounds
D	drag, pounds
M	pitching moment, foot-pounds
C_L	lift coefficient (L/qS_w)
C_D	drag coefficient (D/qS, where S is reference area equal to wing area unless otherwise noted)
C_m	pitching-moment coefficient (M/qS_wc)
L/D	lift-drag ratio
$(L/D)_{max}$	maximum lift-drag ratio
$C_{L_{max}}$	maximum lift coefficient
$C_{L(L/D)_{max}}$	lift coefficient at which lift-drag ratio is a maximum
$C_{D_{o_w}}$	wing profile drag coefficient
$C_{D_{o_{ep}}}$	end-plate profile drag coefficient based on end-plate area
$C'_{D_{o_{ep}}}$	end-plate profile drag coefficient based on wing area
ΔC_D	incremental interference drag coefficient due to juncture between wing and end plates
C_{D_p}	parasite drag coefficient (assumed to be drag coefficient representing any component parts of an airplane other than wing and end plates, such as a fuselage)
q	free-stream dynamic pressure, pounds per square foot $\left(\frac{1}{2}\rho V^2\right)$
ρ	mass density of air, slugs per cubic foot
V	free-stream velocity, feet per second
S_w	wing area, square feet

c	wing chord, feet (constant across wing span)
b	wing span, feet
S_{ep}	area of one end plate minus profile area of wing, square feet
S'_{ep}	area directly above and below wing chord of one end plate minus profile area of wing, square feet
h	maximum height of one end plate, feet
A	wing aspect ratio $\left(b^2/S_w\right)$
A_e	effective aspect ratio
E_e	effective edge-velocity correction factor (reference 13)
u	aspect ratio and taper ratio correction factor for induced drag
α	angle of attack of wing, degrees
C_{L_α}	lift-curve slope of finite-span wing $\left(\frac{\partial C_L}{\partial \alpha}\right)$
c_l	section lift coefficient
c_{l_α}	section lift-curve slope $\left(\frac{\partial c_l}{\partial \alpha}\right)$
$\frac{\partial C_{D_i}}{\partial C_L^2}$	slope of curve of induced-drag coefficient as a function of C_L^2
$\frac{dC_m}{dC_L}$	slope of curve of pitching-moment coefficient as a function of C_L (static-longitudinal-stability parameter)

MODEL AND APPARATUS

A stainless-steel wing was tested alone and in combination with 15 end plates of various areas and shapes in the 6- by 6-foot test section of the Langley stability tunnel. The wing was unswept and untapered and had a span of 32 inches, an aspect ratio of 4, and an NACA 64_1A412 airfoil section.

The end plates have been designated herein by the capital letters A to O. The geometric characteristics and principal dimensions of these end plates are presented in figure 1. End plates A to D were constructed from stainless steel 1/4 inch thick. End plates E to N were constructed from $\frac{1}{4}$-inch plywood and end plates O were shaped from a $\frac{5}{16}$-inch sheet of mahogany. All the wooden end plates were sanded and shellacked to give a smooth surface. The plan-form shapes of end plates A, B, and D were derived by utilizing the calculated pressure field about an infinite-span airfoil having an NACA 64_1A412 airfoil section and operating at zero angle of attack. Points of equal static pressure were used to define the three shapes. The contour of end plate A represents approximately a static-pressure variation of 20 percent with free-stream static pressure, end plate B represents a 10-percent variation, and end plate D represents a 5-percent variation. The pressure field was computed by the method used in reference 7. As designed, the areas of the three end plates cover various amounts of the pressure field about the airfoil.

All the end plates except I and O had rounded leading and trailing edges. End plates I had rounded leading edges and sharp trailing edges so as to simulate an airfoil shape in cross section. The profiles of end plates O represented half of the NACA 0006 airfoil with the flat surfaces inward and the convex surfaces on the outside. Details of the wing and end-plate profiles along with a table of ordinates for the wing are presented in figure 2. For the end plates with their areas all above the wing, the lower edge of each plate was made to coincide with the lower surface of the airfoil and was not rounded. A similar condition existed for the end plates with their areas all below the wing. The top and bottom edges of all the rectangular plates were not rounded. A photograph of one of the wing-end-plate configurations mounted in the tunnel test section is presented as figure 3.

TESTS AND CORRECTIONS

The tests were conducted at a dynamic pressure of 64.3 pounds per square foot, which corresponds to a Mach number of 0.211 and a Reynolds number of approximately 1×10^6.

The model was tested with and without the various end plates attached through an angle-of-attack range from -6° to beyond the angle of maximum lift. Tare tests were conducted on the plain wing and the interference increments thus obtained were applied to all the test data. In addition, the test data were corrected for jet-boundary effects. No corrections, however, were applied for turbulence or blocking.

SCOPE

The results of the investigation presented herein are essentially divided into two parts - "Test Results" and "Generalized Analysis." The part entitled "Test Results" is concerned with the basic data and the determination of experimental values for the various aerodynamic characteristics under consideration. Also included in this section are the effects of several end-plate variables on the experimental values obtained. The part entitled "Generalized Analysis" is concerned mainly with the means of calculating several of the aerodynamic characteristics. Comparisons of the calculated and experimental results are presented; and, in addition, a theoretical analysis of L/D and $(L/D)_{max}$ is included to indicate the effect of varying the factors that influence these two characteristics.

TEST RESULTS

General Remarks

From the data obtained from the wind-tunnel tests, experimental values for the aerodynamic characteristics C_{L_α}, $\frac{\partial C_{D_i}}{\partial C_L^2}$, $\frac{dC_m}{dC_L}$, $C_{L_{max}}$, L/D, $(L/D)_{max}$, and $C_{L_{(L/D)_{max}}}$ were evaluated. It is desirable to know to what extent each of these characteristics is affected by the addition of end plates to the wing and what variations in the end plates themselves produce changes in the values of these characteristics. Some of the end-plate variations which may influence the aerodynamic characteristics are (1) end-plate profile (cross section), (2) end-plate plan form (shape), (3) location of end-plate area with respect to the wing chord line (symmetrical, all above, or all below), and (4) end-plate area. These end-plate variations are discussed in this section of the paper and apply for the most part to end plates having their area distributed over the entire wing chord. The effects of using partial end plates (end plates having their area distributed over only a portion of the wing chord) and end plates extending beyond the wing leading and trailing edges are discussed in the part of the paper entitled "Generalized Analysis."

Basic Data

The lift, drag, and pitching-moment characteristics for the wing alone and in combination with the various end plates are presented in figures 4 and 5. The data exhibit the usual characteristics associated

with end plates, such as an increase in C_{L_α} and $C_{L_{max}}$ and a reduction in the drag coefficient at all lift coefficients above a certain minimum. Below this minimum, the drag coefficient indicates an increase over that of the basic wing. In this low-lift-coefficient range, however, the additional drag due to the end plates is greater than any reduction in the induced drag that they may produce. The lift coefficient at which the beneficial effects of the end plates first begin to occur appears to be a function of end-plate area. These lift coefficients for the various wing-end-plate combinations tested vary over a range from 0.35 to 0.64, the higher lift coefficients being associated with the larger end-plate areas.

All the end-plate configurations tested produced an increase in C_{L_α} and $C_{L_{max}}$ of the basic wing. The end-plate influence on these two characteristics is discussed in the following sections of the paper and can be neglected here.

The static longitudinal stability characteristics of the various wing-end-plate combinations show a slight variation from the stability characteristics of the wing alone. The wing with the various symmetrical end plates attached shows a slight increase in stability over the basic wing. The wing in combination with the end plates having their area all above the wing, with the exception of end plates J, exhibits less stability than the basic wing. Although the percentage changes are large, the absolute value for each separate configuration is small and does not appear to be important.

Figure 6 presents the experimental values of L/D for the wing alone and in combination with the various end plates as a function of C_L. A comparison of the data indicates that all the configurations with end plates produced a much lower value of $(L/D)_{max}$ than the wing alone. The addition of end plates also increased the lift coefficient at which the maximum value of L/D occurred and produced values of L/D at or near the maximum over a wider lift-coefficient range.

Experimental values for all the aerodynamic characteristics under consideration are available from the figures previously discussed except for the slope of the induced-drag curve $\frac{\partial C_{D_i}}{\partial C_L^2}$. In order to obtain values for $\frac{\partial C_{D_i}}{\partial C_L^2}$, a reduction of the drag data presented in figure 5 is required. The procedure followed was to subtract the wing profile drag coefficient from the experimental drag coefficients of the wing-end-plate configurations tested $\left(C_D - C_{D_{ow}}\right)$ at various values of C_L. The drag coefficients

remaining after completing this operation were then plotted against C_L^2 (fig. 7). The slopes of the resulting curves represent $\frac{\partial C_{D_i}}{\partial C_L^2}$.

Subtracting the wing profile drag coefficient was necessary since it varied with lift coefficient. Airfoil section data are not available as yet for the NACA 64_1A412 section; however, the wing profile drag coefficient was obtained by calculating the induced drag for an aspect-ratio-4 airfoil and subtracting it from the experimental data for the wing alone. The expression used for the induced drag was $\frac{C_L^2}{\pi A u}$, where u is the correction factor for aspect ratio and taper ratio and can be obtained from reference 8. A comparison of the wing profile drag coefficient calculated in this manner with the section drag characteristics of an NACA 64_1-412 airfoil section (reference 9) at a Reynolds number of 1×10^6 is presented in figure 8. The figure indicates that the values are in fairly good agreement except at the higher lift coefficients. Some variation is apparent in the values of $C_{D_{o_w}}$ in the region of the drag bucket and in the range of lift coefficients covered by the drag bucket. These two variations, however, are believed to be the result of a small amount of turbulence present in the air stream of the Langley stability tunnel. The two airfoil sections are identical except that the NACA 64_1-412 has a small trailing-edge cusp, whereas the NACA 64_1A412 has the cusp removed.

No attempt was made in the previous calculations to remove the drag of the end plates. The end-plate drag was believed to be fairly independent of lift coefficient and hence would not materially affect the slopes of the curves in the low- and medium-lift-coefficient range. The linear variation obtained for $C_D - C_{D_{o_w}}$ below a C_L^2 of 0.35 (see fig. 7) for all the wing-end-plate configurations enabled the determination of $\frac{\partial C_{D_i}}{\partial C_L^2}$. Figure 7 also indicates that $\frac{\partial C_{D_i}}{\partial C_L^2}$ varies with the end plates tested and apparently is a function of end-plate area (for example, compare the wing with end plates F, G, and H).

Experimental values for the various aerodynamic characteristics of each of the wing-end-plate configurations tested were obtained from the figures previously discussed and are listed in table I.

Effect of End-Plate Profile

The effect of end-plate profile or cross section on the aerodynamic characteristics of wing-end-plate configurations can be obtained by comparing the experimental results for the wing with end plates G and I attached. End plates G and I vary only in the shape of the end-plate cross section. End plates G have rounded leading and trailing edges whereas end plates I were constructed with rounded leading edges and sharp trailing edges so as to simulate an airfoil cross section (fig. 2). Most of the influence of end-plate profile would be expected to occur in the drag. A comparison of the drag characteristics for the two configurations (see fig. 5) indicates that the wing with end plates I has the reduction in the drag with respect to the wing alone occurring at a lower lift coefficient than the wing with end plates G. In addition, the wing with end plates I has a smaller increase in the drag coefficient with respect to the wing alone for the low-lift-coefficient range. If only for the improvement in the drag coefficient, the simulated airfoil-shaped end plates have proved their superiority. End plates I also affected L/D and provided a slightly higher value of $(L/D)_{max}$ than was obtained with end plates G. The values of $\frac{\partial C_{D_i}}{\partial C_L^2}$ and $C_{L(L/D)_{max}}$ were slightly lower for the wing with end plates I.

A similar indication can be obtained by comparing the drag polars for the wing with end plates K and O (fig. 5). The end plates vary only slightly in shape and area; however, an exact comparison cannot be made as in the case of end plates G and I because end plates O extended beyond the wing leading and trailing edges and end plates K did not. Nevertheless, the beneficial effect of using an airfoil section for the end-plate profile is apparent.

The results of these comparisons clearly indicate that using airfoil shapes as end-plate cross sections is highly desirable. This fact was also pointed out in reference 2.

Effect of End-Plate Area

Two series of end plates are available for indicating the effect of end-plate area on the aerodynamic characteristics of wing-end-plate configurations. End plates F, G, and H, which comprise one series, have the same location of end-plate area relative to the wing chord line, the same plan form, and the same cross section; only the end-plate area is varied. These particular end plates seem to be the most logical choice for indicating the effects of end-plate area. Since the chord

for each of these particular end plates is equal to the wing chord, the increase in area is obtained by actually increasing the end-plate height. Increasing the area in this manner, as is indicated subsequently, appears to be the most logical way of increasing the end-plate effect. The other series, consisting of end plates A, B, and D, has essentially the same end-plate cross section; however, the location of the area with respect to the wing chord line, the plan form, and the end-plate area are all dependent on the calculated static-pressure variation chosen for the particular end plate (see section entitled "Model and Apparatus").

Both series of end plates are indicated in figure 9, which presents the experimental results of the effect of end-plate area on the aerodynamic characteristics C_{L_α}, $\frac{\partial C_{D_i}}{\partial C_L^2}$, $C_{L_{max}}$, $(L/D)_{max}$, and $C_{L_{(L/D)_{max}}}$ as a function of S_{ep}/S_w. Increasing the end-plate area provides an increase in C_{L_α}, $C_{L_{max}}$, and $C_{L_{(L/D)_{max}}}$ and a decrease in $\frac{\partial C_{D_i}}{\partial C_L^2}$ and $(L/D)_{max}$. Both series of end plates indicate the same trends for each of the aerodynamic characteristics; however, the calculated shapes show more favorable values for C_{L_α}, $\frac{\partial C_{D_i}}{\partial C_L^2}$, and $(L/D)_{max}$ than the rectangular shapes. Only a slight decrease is apparent in $C_{L_{(L/D)_{max}}}$ for the calculated shapes at the larger end-plate areas and the influence on $C_{L_{max}}$ appears to be negligible. In general, the calculated shapes seem to provide slightly more favorable results; however, the improvement obtained does not seem sufficient to warrant a departure from the more simple geometric shapes.

Effect of End-Plate Plan Form and Location of End-Plate Area Relative to the Wing Chord Line

The effect of end-plate plan form and location of end-plate area with respect to the wing chord line on the aerodynamic characteristics of wing-end-plate configurations can be seen in figure 10. All the end plates presented in this figure have approximately the same area and essentially the same cross section; that is, rounded leading and trailing edges. In addition, the end-plate area was distributed over the entire wing chord but was not permitted to extend beyond the wing leading and trailing edges.

A comparison of experimental results for the wing with end plates G, J, and M attached indicates that the effect of the location of end-plate area relative to the wing chord line is small; however, a very slight advantage in C_{L_α}, $\frac{\partial C_{D_i}}{\partial C_L^2}$, and $C_{L_{max}}$ can be gained by locating the end-plate area all above rather than all below the wing chord line. The variation among the aerodynamic characteristics for end plates G, J, and M is small enough so that the actual choice of the location of the end-plate area relative to the wing chord line can be based on other considerations, such as the end-plate bending moment about the point of attachment, rather than on the aerodynamic characteristics presented herein.

The effect of end-plate plan form can be illustrated best, at least for the particular end plates tested, by comparing the aerodynamic characteristics for the wing with end plates E, G, K, and L attached. Figure 10 indicates that the values for C_{L_α}, $C_{L_{max}}$, and $C_{L_{(L/D)_{max}}}$ are relatively unaffected by the difference in the end-plate shapes indicated here. Most of the variation appears in $\frac{\partial C_{D_i}}{\partial C_L^2}$, which of course affects $(L/D)_{max}$. The influence of the shape on the induced drag has been suggested in reference 2. A comparison of the values of $\frac{\partial C_{D_i}}{\partial C_L^2}$, especially those for end plates K and L, suggests that concentrating the area near the wing trailing edge may be more effective in reducing the induced drag than concentrating the area near the leading edge.

For the aerodynamic characteristics obtained, the actual advantage of using one end plate instead of another is slight. The end plates indicated here do not have enough variety in plan-form shape to permit an actual evaluation of the plan-form effect; however, figure 10 is sufficient to indicate that the effect of end-plate plan form on these aerodynamic characteristics is secondary, as would be expected, and that the dominating factor is by far the end-plate area.

GENERALIZED ANALYSIS

Basic Considerations

Most of the previous investigations of the effects of end plates attached to the tips of unswept wings have been concerned mainly with the increase in lift-curve slope and the reduction in the induced drag. The usual approach to the problem has been to express these two effects by the concept of an effective aspect ratio. The classical theory (reference 3) utilizes the method of conformal transformation applied to the induced drag of the wing with end plates and has resulted in a solution which indicates that the end plates may be considered to cause an increase in the aspect ratio of the basic wing to an extent determined by the ratio of the end-plate height to wing span. A theoretical solution presented in reference 4 is similar to the classical theory; however, an approximate method is employed in the use of the conformal transformation and the solution is obtained as a function of several parameters, such as the ratio of the end-plate height to wing span, the ratio of the end-plate height above the wing chord to the height below the chord, and the ratio of the height above the chord to the wing semispan.

As a result of the nature of both solutions, the distribution of end-plate area along the wing chord is neglected. An exact solution would undoubtedly show that the area distribution had some effect. A comparison of the two solutions indicates that almost identical predictions of the effective aspect ratio will result for a given value of the ratio of end-plate height to wing span. It should be pointed out that the solution of reference 4 is based on the condition of minimum induced drag, and a theoretical study of tail assemblies (reference 10) indicates that for certain configurations this assumption may lead to excessively high values of the ratio A_e/A. For the particular case of wings with end plates, where the end-plate height is small relative to the wing span, the assumption appears to incur little or no error.

The more general attempts for the solution of the end-plate effects, such as reference 5, are based on the empirical result that only the end-plate area is of importance. These solutions attempt to correlate the ratio A_e/A with such parameters as S_{ep}/S_w and $\sqrt{S_{ep}}/b$. For convenience these parameters may be considered as the ratio of an effective end-plate height to wing span. For example, $\sqrt{S_{ep}}$ may be considered as the height of a square having an area of S_{ep}. An effective end-plate height obtained by dividing the end-plate area directly above and below the wing chord by the wing chord has also been considered.

Several of these parameters were used as a basis for correlation of the data presented herein. Values of the different parameters for each of the end plates tested are presented in table II. The parameter chosen as the most representative for a wide range of end-plate plan forms was $\sqrt{S'_{ep}}/b$, where S'_{ep} is defined as the projected area of one end plate directly above and below the wing chord minus the profile area of the wing. Limiting the area to that located directly above and below the wing chord was necessary in order to obtain a reasonable prediction for the wing with end plates N attached. Subtracting the profile area of the wing permits the ratio A_e/A to have the value 1.0 for the wing alone or, in other words, when the end-plate parameter equals zero. If the wing profile area were not subtracted, the ratio A_e/A would have to become equal to 1.0 at some value of the end-plate parameter greater than zero and dependent on the profile area of the wing.

Effective Aspect Ratio

Determination by lift-curve slope.- The end-plate effect on C_{L_α} is usually expressed as an increase in the aspect ratio of the basic wing, the amount of the increase depending on some geometric characteristic of the end plates. Hence, to obtain a reasonable prediction of C_{L_α} for a finite-span unswept wing with end plates requires a wing theory that will predict fairly accurate values of C_{L_α} over a wide range of wing aspect ratios. Probably the most familiar wing theory is the lifting-line theory which expresses the lift-curve slope in the following manner:

$$C_{L_\alpha} = \frac{c_{l_\alpha}}{1 + \frac{57.3c_{l_\alpha}}{\pi A}}$$

The results predicted by this theory, however, have been known to be inaccurate for low-aspect-ratio wings. Robert T. Jones (reference 11) developed a theoretical correction which he applied to the lifting-line expression. This correction, commonly referred to as the Jones edge-velocity correction, gives only about two-thirds of the total theoretical correction required. Swanson and Crandall (reference 12) have obtained an effective edge-velocity correction by modifying the Jones edge-velocity correction with lifting-surface results obtained from an electromagnetic-analogy method on elliptical plan forms. The modified

equation can be expressed as follows:

$$C_{L_\alpha} = \frac{c_{l_\alpha}}{E_e + \frac{57.3c_{l_\alpha}}{\pi A}}$$

where E_e is the effective edge-velocity correction and can be obtained from reference 13. Although the corrections were developed for elliptic wings, the results for plan forms other than elliptical have been found to be fairly accurate over the aspect-ratio range.

Figure 11 presents the results for C_{L_α} determined by the modified equation as a function of aspect ratio for a section lift-curve slope of 0.108. This particular value for c_{l_α}, determined from the modified equation by using the experimental C_{L_α} for the wing alone and the wing aspect ratio, is almost identical to the c_{l_α} for an NACA 64_1-412 airfoil section given in reference 9. Values of the effective aspect ratio for the various wing-end-plate configurations were determined by using the experimental lift-curve slopes and figure 11. The results are presented in ratio form A_e/A in figure 12 as a function of several end-plate parameters.

The A_e/A values, expressed as a function of h/b, indicate fairly good agreement with the classical theory over the complete h/b range. However, it would seem that in predicting A_e/A for a wing-end-plate configuration where the end plates are of unusual plan form, a more representative parameter such as some function of the end-plate area should be used. Several area parameters were tried as indicated in figure 12. Correlating the A_e/A values with S_{ep}/S_w and comparing the results with the classical theory in which the ratio S_{ep}/S_w is interpreted as an effective value of h/b indicates that a very poor agreement exists for the smaller end-plate areas and for end plates N. When the parameter $\frac{S'_{ep}/c}{b}$ is used, a much better agreement is obtained for end plates N; however, for the particular end plates tested, this parameter provided a change in the values of end plates D, N, and O only. For the smaller end-plate areas, the use of $\sqrt{S_{ep}}/b$ appears to give somewhat better agreement with the classical theory than the previous

area parameters; however, end plate N now appears rather poor. The form $\sqrt{S'_{ep}}/b$ appears to combine the advantages of both $\frac{S'_{ep}/c}{b}$ and $\sqrt{S_{ep}}/b$. For the parameters $\sqrt{S'_{ep}}/b$ and $\sqrt{S_{ep}}/b$ the prediction developed from reference 5, which is applicable only for a wing of aspect ratio 4, is not in good agreement with the data and indicates much lower values of A_e/A than were obtained. The experimental values of A_e/A make the classical theory appear to underestimate the end-plate effect; however, this underestimation need not be true. It should be pointed out that the values obtained for A_e, and hence the ratios of A_e/A, are critically dependent on the value of C_{L_α} for the wing alone. Increasing C_{L_α} from 0.065, which was used herein, to 0.067 will shift the experimental values as functions of $\sqrt{S'_{ep}}/b$ downward until the classical theory would appear to be an average curve. For each wing-end-plate combination the A_e/A value is also critically dependent on the lift-curve slope of the configuration tested. This dependence can be seen in figure 11, which indicates that large values of A_e/A can result for only a small increase in C_{L_α} for the particular wing aspect ratio under investigation. Some scatter of the experimental values for a given value of $\sqrt{S'_{ep}}/b$ is apparent; however, the scatter is probably the result of neglecting the distribution of end-plate area along the wing chord and the location of the area relative to the wing chord line.

Determination by induced drag.- Since most theoretical solutions on end-plate effects are based on a consideration of the reduction in the induced drag of the wing, using the concept of an effective aspect ratio, the values for A_e of the various wing-end-plate configurations were obtained from the slopes of the drag curves $\left(C_D - C_{D_{o_w}} \text{ against } C_L^2\right)$ presented in figure 7. The slopes represent $\frac{\partial C_{D_i}}{\partial C_L^2}$ which is essentially $1/\pi A_e$, and A_e can then either be calculated or obtained from figure 11. The correction factor for aspect ratio and taper ratio has been neglected in this determination since the effect of this factor on the various values of A_e is small. In the determination of A_e for other configurations of wings and end plates, this factor should be considered.

Values of A_e obtained in this manner and expressed as the ratio A_e/A are presented in figure 13 as functions of the same

end-plate parameters as were used for the correlation of A_e/A determined from the experimental lift-curve slopes. For each of the end-plate parameters, the experimental values of A_e/A determined from $\frac{\partial C_{D_i}}{\partial C_L^2}$ show a much better agreement with the classical theory than the corresponding A_e/A values obtained from the experimental values of C_{L_α}. Essentially the same reason applies here for wanting to express the end-plate parameter as some function of end-plate area as applied for the lift-curve slope; however, the apparent advantage of varying the parameter is much less than for the lift-curve slope analysis. Nevertheless, since the same theory is used to predict the end-plate effects on both characteristics, the same parameter must be used for both. It is apparent that none of the area parameters provide as good an agreement between the experimental data $\left(\text{determined from both } C_{L_\alpha} \text{ and } \frac{\partial C_{D_i}}{\partial C_L^2}\right)$ and the theory as does the parameter h/b. However, the parameter $\sqrt{S'_{ep}}/b$ will be used in the remaining sections of the paper since it is believed to be more applicable to a wider range of end-plate plan forms than were tested. The empirical solution developed from reference 5, which is applicable only for an aspect-ratio-4 wing, is in very poor agreement with the data determined from both the lift-curve slopes and the induced drag and indicates much lower values for A_e/A than were obtained.

The parameter $\sqrt{S'_{ep}}/b$ used to correlate the theoretical A_e/A values with the experimental results determined from both C_{L_α} and $\frac{\partial C_{D_i}}{\partial C_L^2}$ essentially means that the end-plate area extending beyond the wing leading and trailing edges is relatively ineffective in producing an increase in the effective aspect ratio. It should be noted that partial end plates, that is, end plates having their areas distributed over only part of the wing chord, have not been considered in this investigation. The results of reference 2, however, indicate that partial end plates should be less effective than end plates having their areas distributed over the complete wing chord. The basis of comparison in this reference was the drag polar, but the influence will also be noticed on L/D and $(L/D)_{max}$.

Development of Equations

Using the concept of an effective aspect ratio to predict the induced drag of the wing when end plates are attached makes possible the development of expressions for the end-plate effects on L/D, $(L/D)_{max}$, and $C_{L_{(L/D)_{max}}}$. The expressions as developed apply not only to a wing-end-plate configuration but also to wing-body combinations or complete airplanes with end plates attached. The total drag coefficient of such configurations can be expressed as follows:

$$C_D = C_{D_{o_w}} + \frac{C_L^2}{\pi A_e} + 2C_{D_{o_{ep}}} \frac{S_{ep}}{S_w} + \Delta C_D + C_{D_p} \tag{1}$$

where $C_{D_{o_w}}$, $C_L^2/\pi A_e$, ΔC_D, and C_{D_p} are based on wing area and $C_{D_{o_{ep}}}$ is based on end-plate area. The effect of a fuselage or other component parts of a complete airplane other than the wing and end plates is contained in the term C_{D_p}. For a wing-end-plate configuration, therefore, C_{D_p} would be zero. It should be pointed out that any possible thrust effect arising from a consideration of the loading imposed on the end plates by the presence of the wing is neglected.

The lift-drag ratio can then be written as

$$\frac{L}{D} = \frac{C_L}{C_{D_{o_w}} + \frac{C_L^2}{\pi A_e} + 2C_{D_{o_{ep}}} \frac{S_{ep}}{S_w} + \Delta C_D + C_{D_p}} \tag{2}$$

In order to extend this expression to obtain $(L/D)_{max}$, the lift coefficient at which the value for L/D becomes a maximum must first be determined. This lift coefficient can be obtained by setting the first derivative of D/L with respect to C_L equal to zero. This procedure yields

$$\frac{C_L^2}{\pi A_e} = C_{D_{o_w}} + 2C_{D_{o_{ep}}} \frac{S_{ep}}{S_w} + \Delta C_D + C_{D_p}$$

Solving for C_L, which is now $C_{L_{(L/D)_{max}}}$, gives

$$C_{L_{(L/D)_{max}}} = \sqrt{\pi A_e \left(C_{D_{o_w}} + 2C_{D_{o_{ep}}} \frac{S_{ep}}{S_w} + \Delta C_D + C_{D_p}\right)} \tag{3}$$

Now, $(L/D)_{max}$ can be expressed as

$$\left(\frac{L}{D}\right)_{max} = \frac{C_{L_{(L/D)_{max}}}}{\frac{2\left[C_{L_{(L/D)_{max}}}\right]^2}{\pi A_e}} = \frac{\pi A_e}{2C_{L_{(L/D)_{max}}}} \tag{4}$$

or

$$\left(\frac{L}{D}\right)_{max} = \frac{1}{2}\sqrt{\frac{\pi A_e}{C_{D_{o_w}} + 2C_{D_{o_{ep}}} \frac{S_{ep}}{S_w} + \Delta C_D + C_{D_p}}} \tag{5}$$

Calculations of the aforementioned characteristics should be made by use of the most accurate values of the various terms available. The variation of $C_{D_{o_w}}$ with C_L should be used in calculating L/D if accurate results at higher lift coefficients are to be obtained. However, using the minimum $C_{D_{o_w}}$ is believed to be of sufficient accuracy to yield reasonable values for $(L/D)_{max}$ and $C_{L_{(L/D)_{max}}}$. The parasite-drag term C_{D_p} may vary widely for different configurations and, as a result, values would probably have to be obtained from experimental data if accurate values of L/D and $(L/D)_{max}$ are desired. The correction factor for aspect ratio and taper ratio has been neglected in the previous expressions since less than a 1-percent error will result for aspect ratios between 0 and 6 and taper ratios between 0.3 and 1.0.

End-Plate Drag

In order to make an estimate of L/D, $(L/D)_{max}$, or $C_{L_{(L/D)_{max}}}$ for the wing-end-plate configuration, reasonable values for the various drag terms appearing in the expressions must be determined. The wing profile drag coefficient $C_{D_{o_w}}$ can usually be obtained from known section characteristics; however, evaluating $C_{D_{o_{ep}}}$ and ΔC_D is more difficult

and a reduction of the experimental data was resorted to in order to obtain average values. The results of this reduction are presented in figures 14 and 15. When the end-plate profile drag coefficient is based on end-plate area, $C_{D_{o_{ep}}}$ would apparently depend only on the end-plate profile and would probably be high for the end plates with the blunt trailing edges. Since the end-plate angle of attack is merely the angle induced by the loading imposed on the end plates owing to the presence of the wing, any variation of $C_{D_{o_{ep}}}$ with lift coefficient can be neglected. For this analysis ΔC_D was also assumed to be independent of C_L and, in addition, should be almost independent of end-plate profile and end-plate area, at least above a certain minimum for the end-plate area.

The actual reduction of the experimental data was performed in the following manner. The drag coefficient of the plain wing was subtracted from the drag coefficients of the wing with the various end plates attached for the condition of zero lift (fig. 5). This particular condition was chosen so that the induced-drag term would be zero. The result should be $C'_{D_{o_{ep}}} + \Delta C_D$, where $C'_{D_{o_{ep}}}$ is based on wing area. Figure 14 presents this increment as a function of S_{ep}/S_w. The data appear to have some scatter; however, the variation would be expected to be linear for all values of S_{ep}/S_w above a certain minimum. With the assumed variation, a value of 0.002 for S_{ep}/S_w equal to zero still remains and this increment represents ΔC_D, where ΔC_D is based on the wing area and would be constant for all wing-end-plate configurations having S_{ep}/S_w above some minimum value.

Subtracting this value (0.002) from the experimental results for $C'_{D_{o_{ep}}} + \Delta C_D$ and basing the end-plate profile drag coefficient obtained on end-plate area $\left(C_{D_{o_{ep}}}\right)$ yields the results presented in figure 15. The scatter of the data is within the range expected for this type of analysis. Of particular interest in figure 15 are the low values for end plates N and O, which may possibly indicate that the interference drag increment ΔC_D might be reduced by allowing the end plate to extend somewhat beyond the leading and trailing edges of the wing. A more complete analysis would very likely indicate that the value of ΔC_D depends also on the location of the end-plate area relative to the wing chord line (all above, all below, or symmetrical) and, for a given wing area, on the wing aspect ratio. However, verification of these effects would require additional end-plate tests.

As previously stated, ΔC_D is believed to be fairly independent of end-plate area, at least above a certain minimum value. Below this

minimum value it obviously must be a function of the end-plate area or some other parameter in which the end-plate area is expressed, such as $\sqrt{S'_{ep}}/b$. Take, for example, the drag expression for the wing-end-plate configuration (included in equation (1)). As the end-plate area approaches the value zero, the drag of the wing-end-plate combination must approach the drag of the wing alone. Therefore, A_e must approach A and $C_{D_{o_{ep}}} \frac{S_{ep}}{S_w}$ must approach zero; hence, ΔC_D must likewise approach zero. Means for evaluating this variation are not available; therefore, the variation of ΔC_D indicated in figure 16 as a function of $\sqrt{S'_{ep}}/b$ was assumed. The upper limit of the variation of ΔC_D with $\sqrt{S'_{ep}}/b$ was chosen at the value of $\sqrt{S'_{ep}}/b$ of 0.15 so that a value of ΔC_D of approximately 0.002 would apply to end plates B and F.

Comparison of Calculated and Experimental Results

A comparison of the calculated and experimental results for the wing alone and in combination with the various end plates is presented in table I and in figures 17 and 18. Calculations were performed for C_{L_α}, $(L/D)_{max}$, $\frac{\partial C_{D_i}}{\partial C_L^2}$, and $C_{L_{(L/D)_{max}}}$ and are compared with experimental values in figure 17. Figure 18 presents the calculated and experimental values of L/D as a function of C_L for the wing in combination with end plates E and F. No attempt was made to calculate $C_{L_{max}}$ for the various configurations tested; however, it is apparent from the experimental values of $C_{L_{max}}$ as a function of $\sqrt{S'_{ep}}/b$ (fig. 17) that some increase in the value of $C_{L_{max}}$ for the basic wing is available through the use of end plates. For end plates having values of $\sqrt{S'_{ep}}/b$ of 0.30 and above, the rate of increase in $C_{L_{max}}$ appears to approach zero.

The calculated curves for C_{L_α} and $\frac{\partial C_{D_i}}{\partial C_L^2}$ as functions of $\sqrt{S'_{ep}}/b$ were obtained by utilizing the classical theory expressing A_e/A as a function of $\sqrt{S'_{ep}}/b$ together with figure 11. These particular curves therefore apply only for aspect-ratio-4 wings. In addition, the calculated curve for C_{L_α} is valid only for a value of c_{l_α} of 0.108. All

the calculated values for the lift-curve slope are within approximately 6 percent of the experimental values. Figure 17 furnishes a much more direct comparison of the end-plate effects on C_{L_α} than does figure 12, where the effective aspect ratio is expressed as a function of $\sqrt{S'_{ep}}/b$ as determined from the experimental lift-curve slopes. Large variations can apparently exist in the evaluation of A_e/A without producing much of a variation in C_{L_α}. It should be noted (fig. 11) that even a larger variation in A_e/A can be tolerated for aspect ratios greater than 4; however, for aspect ratios less than 4, the opposite is true.

The variation between the calculated and experimental values for $\frac{\partial C_{D_i}}{\partial C_L{}^2}$ (fig. 17) indicates that the error in predicting this aerodynamic characteristic is approximately twice as large as for the lift-curve slope. This difference is expected, however, since the drag is inversely proportional to A_e. The variations obtained between the calculated and experimental values of C_{L_α} and $\frac{\partial C_{D_i}}{\partial C_L{}^2}$ are considered to be within the range of accuracy expected for this type of analysis.

The values of the various drag terms used in the calculation of $(L/D)_{max}$ have been given previously; however, the calculated curve applies only to the wing-end-plate configurations in which the end-plate area is located directly above and below the wing chord. Limiting the area in this manner makes it possible to utilize the relationship

$$\frac{S_{ep}}{S_w} = A\left(\frac{\sqrt{S'_{ep}}}{b}\right)^2$$

Now, only a value for $\sqrt{S'_{ep}}/b$ is required to evaluate A_e, $C_{D_{o_{ep}}}\frac{S_{ep}}{S_w}$, and ΔC_D which appear in equation (5). The condition where this relationship does not hold corresponds to end plates having their area extending beyond the leading and trailing edges, for which any number of values of S_{ep}/S_w can correspond to a given value of $\sqrt{S'_{ep}}/b$. The particular calculated curve indicated applies for 11 of the end plates tested, excluding only end plates D, I, N, and O. End plates I, although the area is located directly above and below the wing chord, must be excluded

since the profile drag coefficient for these particular end plates is considerably less than 0.015 (see fig. 15). A comparison of the calculated curve and experimental values (fig. 17) indicates a fair amount of scatter; however, the value of $(L/D)_{max}$ for most of the wing-end-plate combinations can be predicted within 10 percent of the experimental values. Some increase in the accuracy could be expected if more representative values for $C_{D_{o_{ep}}}$ and ΔC_D for the various end plates were used; however, methods of predicting A_e limit the accuracy so that consistent predictions cannot be made within an accuracy greater than 5 percent. The value of $C_{D_{o_w}}$ used in the calculations was 0.005, which for this particular section is constant over the low- and medium-lift-coefficient range. In calculating $(L/D)_{max}$ for other wing-end-plate configurations, it is suggested that the minimum profile drag be used for $C_{D_{o_w}}$ since $(L/D)_{max}$ is expected to occur at a relatively low lift coefficient. If a more accurate value is desired, calculating $C_{L_{(L/D)max}}$ and obtaining $C_{D_{o_w}}$ from section data for the corresponding lift coefficient should be of sufficient accuracy for most engineering calculations.

The calculated curve of $C_{L_{(L/D)_{max}}}$ as a function of $\sqrt{S'_{ep}}/b$ (fig. 17) indicates that the scatter of the experimental values with respect to the curve is small; hence, the accuracy of the various terms evaluated herein is sufficient to provide a fairly good estimate for $C_{L_{(L/D)_{max}}}$. The calculated curve indicated is similar to the $(L/D)_{max}$ curve in that it applies only to end plates having their areas directly above and below the wing chord; hence, the limitations indicated for the calculated $(L/D)_{max}$ curve apply here as well. Values of $C_{L_{(L/D)max}}$ in the neighborhood of 0.6 can be obtained for the larger end-plate areas; hence, the value for $C_{D_{o_w}}$ would necessarily have to correspond to this lift coefficient if reasonable values of L/D and $(L/D)_{max}$ are to be obtained.

Calculations were also performed for L/D in order to obtain the variation of L/D with C_L. The calculations were limited to only two of the configurations tested, the wing in combination with end plates E and F. The results are presented in figure 18. The variations of L/D with C_L for the other wing-end-plate configurations are expected to be similar. The calculated values for the wing with end plates E are in good

agreement with the experimental values up to a C_L of 0.5. Above this C_L the calculated values are slightly lower than the experimental points. Calculated values for the wing with end plates F show good agreement at the lower and higher lift coefficients, but the predicted values are slightly higher than the experimental points in the region of $(L/D)_{max}$.

Analysis of L/D and $(L/D)_{max}$ Expressions

The results of an analysis of the $(L/D)_{max}$ expression, developed herein, are presented in figures 19 to 21 for the wing-end-plate configuration $\left(C_{D_p} = 0\right)$. This analysis serves the purpose of indicating whether an increase in the $(L/D)_{max}$ of an unswept wing is attainable by the addition of end plates and, if so, what combinations of $C_{D_{o_w}}$, $C_{D_{o_{ep}}}$, $\sqrt{S'_{ep}}/b$, and A will produce such an increase. The calculations were performed in such a manner that each of the figures 19 to 21 essentially indicates the influence of $\sqrt{S'_{ep}}/b$ and one of the terms $C_{D_{o_w}}$, $C_{D_{o_{ep}}}$, or A on $(L/D)_{max}$. A series of curves, expressing two terms as variables and two as constants, is thereby presented in each figure. Values of 0.0050 and 4 were used for $C_{D_{o_w}}$ and A, respectively, when each of these terms was held constant. These values correspond to the minimum profile drag coefficient and the aspect ratio of the wing tested. A value of 0.0025 was used for $C_{D_{o_{ep}}}$ since figure 19 indicates that the curve for this value produces a smaller deviation from the wing-alone value of $(L/D)_{max}$ over the $\sqrt{S'_{ep}}/b$ range than any of the curves for higher values of $C_{D_{o_{ep}}}$. This particular value for $C_{D_{o_{ep}}}$ probably represents about the lowest value that could be obtained and would correspond to thin airfoil-shaped end plates. Values for A_e were determined from the classical theory and ΔC_D was assumed to vary as indicated in figure 22. This variation of ΔC_D with $\sqrt{S'_{ep}}/b$ is slightly more conservative over the range of $\sqrt{S'_{ep}}/b$ from 0 to 0.30 than the variation used in calculating the values for the various wing-end-plate configurations tested. Hence, the calculations can be considered to correspond to an efficient wing-end-plate combination with respect to drag and should indicate substantial increases in $(L/D)_{max}$ if such increases are obtainable.

For the particular values chosen, figures 19 to 21 indicate that no substantial increases were obtainable in $(L/D)_{max}$ for the wing. Small increases are apparent for the aspect-ratio-4 wing with very efficient end plates $\left(C_{D_{o_{ep}}} = 0.0025\right)$ at the higher values of $C_{D_{o_w}}$

(fig. 20), and even larger increases will apparently occur for an aspect-ratio-2 wing with efficient end plates at the higher values of $C_{D_{o_w}}$. However, for such cases, the absolute value of $(L/D)_{max}$ will, of necessity, be low.

Calculated values of L/D for the wing-end-plate configuration as a function of $\sqrt{S'_{ep}}/b$ for various lift coefficients are presented in figure 23. The values of the various drag terms used in the calculations are the same as those used for determining $(L/D)_{max}$, except that the variation of $C_{D_{o_w}}$ with C_L (fig. 8) was used instead of the minimum-profile-drag value. The results indicate that substantial increases in the value of L/D can be obtained at the higher lift coefficients for a limited range of $\sqrt{S'_{ep}}/b$ but that no increases in the value of $(L/D)_{max}$ are obtainable.

The analysis thus far has been concerned only with the wing-end-plate configuration. The effect on $(L/D)_{max}$ of adding end plates to wing-body combinations or complete airplanes, for which the total drag of components other than the wing and end plates may be large relative to the wing drag, is indicated in figure 24. Values of $C_{D_{o_w}}$, $C_{D_{o_{ep}}}$, and ΔC_D are the same as those used in the analysis of the wing-end-plate configuration. Also included in figure 24 is the effect on $(L/D)_{max}$ of adding the end-plate area to the wing tips, thus increasing the wing span and hence the geometric aspect ratio of the wing. Values of the geometric aspect ratio thus obtained are indicated on the curve for $C_{D_p} = 0.030$ and apply for the remaining curves at the same value of $\sqrt{S'_{ep}}/b$. The results indicate that substantial percentage increases in $(L/D)_{max}$ may be obtained by the use of end plates; however, the increases obtained with end plates having a value of $\sqrt{S'_{ep}}/b$ of 0.2 or higher are not likely to be as large as those which would be obtained by utilizing the end-plate area as a simple addition to the wing span. The use of end plates as a means of improving the maximum lift-drag ratios of wing-body combinations or complete airplanes would seem to be of primary interest when it is desired to keep the wing span as small as possible. Of particular interest in figure 24 is the range of $\sqrt{S'_{ep}}/b$ from 0 to 0.2 where the curves for the end plates attached show slightly higher values of $(L/D)_{max}$ than the curves for the end-plate area added to the wing tips. Owing to the uncertainty of the values of ΔC_D used in the calculations for this range of $\sqrt{S'_{ep}}/b$, the increase may or may not actually exist. It is sufficient, however, to note that even if the increases are present the values will probably be small and hence can be considered negligible.

The analyses presented in figures 19 to 21, 23, and 24 are for a range of $\sqrt{S'_{ep}}/b$ from 0 to 1.0. The results of reference 10 suggest that the theory used herein to predict A_e/A at the higher values of $\sqrt{S'_{ep}}/b$ leads to an overprediction of A_e and hence somewhat higher values of L/D and $(L/D)_{max}$ than would be attainable.

CONCLUSIONS

The results of the wind-tunnel investigation and an analysis of the effects of end plates on the aerodynamic characteristics of an unswept wing indicated the following conclusions:

1. The addition of end plates to an unswept wing may provide relatively large increases in the lift-drag ratio at the higher lift coefficients for a limited range of end-plate areas, but end plates cannot be expected to produce substantial increases in the maximum lift-drag ratio. The most favorable effect of end plates on the maximum lift-drag ratio is obtained when the wing aspect ratio is low and the ratio of the wing profile drag coefficient to end-plate profile drag coefficient is high. For such cases, however, the absolute value of the maximum lift-drag ratio will, of necessity, be low.

2. Substantial increases may be obtained in the maximum lift-drag ratio of wing-body combinations or complete airplanes, for which the total drag of the components other than the wing is large relative to the wing drag, by the use of appropriately designed end plates. Except possibly for the smaller end-plate areas, however, the increases obtained are not likely to be as large as those which would be obtained by utilizing the end-plate area as a simple addition to the wing span, thus increasing the wing geometric aspect ratio.

3. The lift coefficient at which the lift-drag ratio became a maximum increased with an increase in end-plate area. Adding end plates to the wing also tended to increase the lift-coefficient range at which the lift-drag ratio remained at or near the maximum value.

4. The maximum lift coefficient of the wing experienced an increase when the end plates were added. The rate of increase, however, decreased with increasing end-plate area.

5. The lift-curve slope for the wing-end-plate combinations investigated, as well as the slope of the curve of induced-drag coefficient as a function of the lift coefficient squared, could be calculated within reasonable accuracy by using the classical theory for evaluating the end-plate effects.

6. The use of airfoil shapes as end-plate cross sections is desirable.

7. The influence of the addition of end plates of various sizes and shapes on the static longitudinal stability of an unswept wing was found to be negligible.

Langley Aeronautical Laboratory
National Advisory Committee for Aeronautics
Langley Field, Va., May 2, 1951

REFERENCES

1. Reid, Elliott G.: The Effects of Shielding the Tips of Airfoils. NACA Rep. 201, 1924.

2. Hemke, Paul E.: Drag of Wings with End Plates. NACA Rep. 267, 1927.

3. Von Kármán, Th., and Burgers, J. M.: General Aerodynamic Theory - Perfect Fluids. Airfoils and Airfoil Systems of Finite Span. Vol. II of Aerodynamic Theory, div. E., ch. IV, sec. 19, W. F. Durand, ed., Julius Springer (Berlin), 1935, pp. 211-212.

4. Mangler, W.: The Lift Distribution of Wings with End Plates. NACA TM 856, 1938.

5. Bates, William R.: Collection and Analysis of Wind-Tunnel Data on the Characteristics of Isolated Tail Surfaces with and without End Plates. NACA TN 1291, 1947.

6. Riebe, John M., and Watson, James M.: The Effect of End Plates on Swept Wings at Low Speed. NACA TN 2229, 1950.

7. Daley, Bernard N., and Hanna, Lillian E.: Subsonic Two-Dimensional-Flow Conditions near an Airfoil Determined by Static Pressures Measured at the Tunnel Wall. NACA TN 1873, 1949.

8. Anderson, Raymond F.: Determination of the Characteristics of Tapered Wings. NACA Rep. 572, 1936.

9. Loftin, Laurence K., Jr., and Smith, Hamilton A.: Aerodynamic Characteristics of 15 NACA Airfoil Sections at Seven Reynolds Numbers from 0.7×10^6 to 9.0×10^6. NACA TN 1945, 1949.

10. Katzoff, S., and Mutterperl, William: The End-Plate Effect of a Horizontal-Tail Surface on a Vertical-Tail Surface. NACA TN 797, 1941.

11. Jones, Robert T.: Theoretical Correction for the Lift of Elliptic Wings. Jour. Aero. Sci., vol. 9, no. 1, Nov. 1941, pp. 8-10.

12. Swanson, Robert S., and Crandall, Stewart M.: Lifting-Surface-Theory Aspect-Ratio Corrections to the Lift and Hinge-Moment Parameters for Full-Span Elevators on Horizontal Tail Surfaces. NACA Rep. 911, 1948. (Formerly NACA TN 1175.)

13. Swanson, Robert S., and Priddy, E. LaVerne: Lifting-Surface-Theory Values of the Damping in Roll and of the Parameter Used in Estimating Aileron Stick Forces. NACA ARR L5F23, 1945.

TABLE I.- SUMMARY TABLE OF EXPERIMENTAL AND CALCULATED VALUES

Symbol	End plate attached	C_{L_α}		$\partial C_{D_i}/\partial C_L^2$		$C_{L_{max}}$	$(L/D)_{max}$		$C_{L_{(L/D)_{max}}}$		Experimental A_e/A from -	
		Experimental	Calculated	Experimental	Calculated	Experimental	Experimental	Calculated	Experimental	Calculated	C_{L_α}	$\frac{\partial C_{D_i}}{\partial C_L^2}$
○	None	0.0650	0.0650	------	0.0798	1.08	23.6	23.9	0.29	0.26	1.00	1.00
□	A	.0712	.0692	0.0710	.0688	1.14	21.1	21.7	.35	.33	1.25	1.13
◇	B	.0758	.0720	.0578	.0620	1.19	21.2	20.0	.42	.40	1.47	1.39
△	C	.0770	.0728	.0612	.0602	1.21	22.2	19.4	.38	.43	1.56	1.31
◿	D	.0810	.0757	.0479	.0535	1.21	18.2	16.2	.50	.58	1.85	1.68
◿	E	.0773	.0740	.0566	.0571	1.19	18.6	18.5	.50	.47	1.57	1.42
◠	F	.0730	.0728	.0683	.0602	1.18	17.9	19.4	.44	.43	1.33	1.18
⬡	G	.0758	.0740	.0608	.0571	1.21	16.4	18.5	.50	.47	1.47	1.32
◇	H	.0805	.0767	.0460	.0518	1.21	16.0	16.4	.60	.59	1.80	1.75
◁	I	.0768	.0740	.0598	.0571	1.17	20.4	18.5	.41	.47	1.54	1.34
▽	J	.0758	.0740	.0550	.0571	1.20	18.1	18.5	.49	.47	1.47	1.46
◸	K	.0775	.0738	.0594	.0578	1.16	17.0	18.7	.53	.46	1.59	1.35
◸	L	.0760	.0738	.0528	.0578	1.18	17.9	18.7	.52	.46	1.50	1.52
◡	M	.0736	.0740	.0584	.0571	1.13	18.2	18.5	.49	.47	1.35	1.38
◡	N	.0735	.0740	.0564	.0571	1.13	19.5	15.7	.47	.56	1.35	1.43
◁	O	.0756	.0732	.0576	.0590	1.18	21.2	18.6	.34	.45	1.48	1.38

NACA

TABLE II.- VALUES OF THE VARIOUS END-PLATE PARAMETERS FOR THE

WING-END-PLATE COMBINATIONS INVESTIGATED

$\left[S_w = 1.77 \text{ sq ft}\right]$

End plate	S_{ep} (sq ft)	S'_{ep} (sq ft)	$\frac{S_{ep}}{S_w}$	$\frac{S'_{ep}/c}{b}$	$\sqrt{S_{ep}}/b$	$\sqrt{S'_{ep}}/b$	h (ft)	h/b
A	0.046	0.046	0.026	0.026	0.080	0.080	0.200	0.075
B	.156	.156	.088	.088	.148	.148	.411	.154
C	.206	.206	.116	.116	.170	.170	.273	.140
D	.619	.507	.348	.285	.295	.266	.921	.345
E	.313	.313	.176	.176	.210	.210	.666	.250
F	.206	.206	.116	.116	.170	.170	.362	.136
G	.661	.661	.176	.176	.210	.210	.523	.197
H	.619	.619	.348	.348	.295	.295	.982	.368
I	.313	.313	.176	.176	.210	.210	.523	.197
J	.314	.314	.177	.177	.210	.210	.510	.192
K	.289	.289	.163	.163	.202	.202	.833	.312
L	.289	.289	.163	.163	.202	.202	.833	.312
M	.314	.314	.177	.177	.210	.210	.542	.203
N	.619	.313	.348	.176	.295	.210	.523	.197
O	.309	.246	.174	.138	.208	.185	.667	.250

NACA

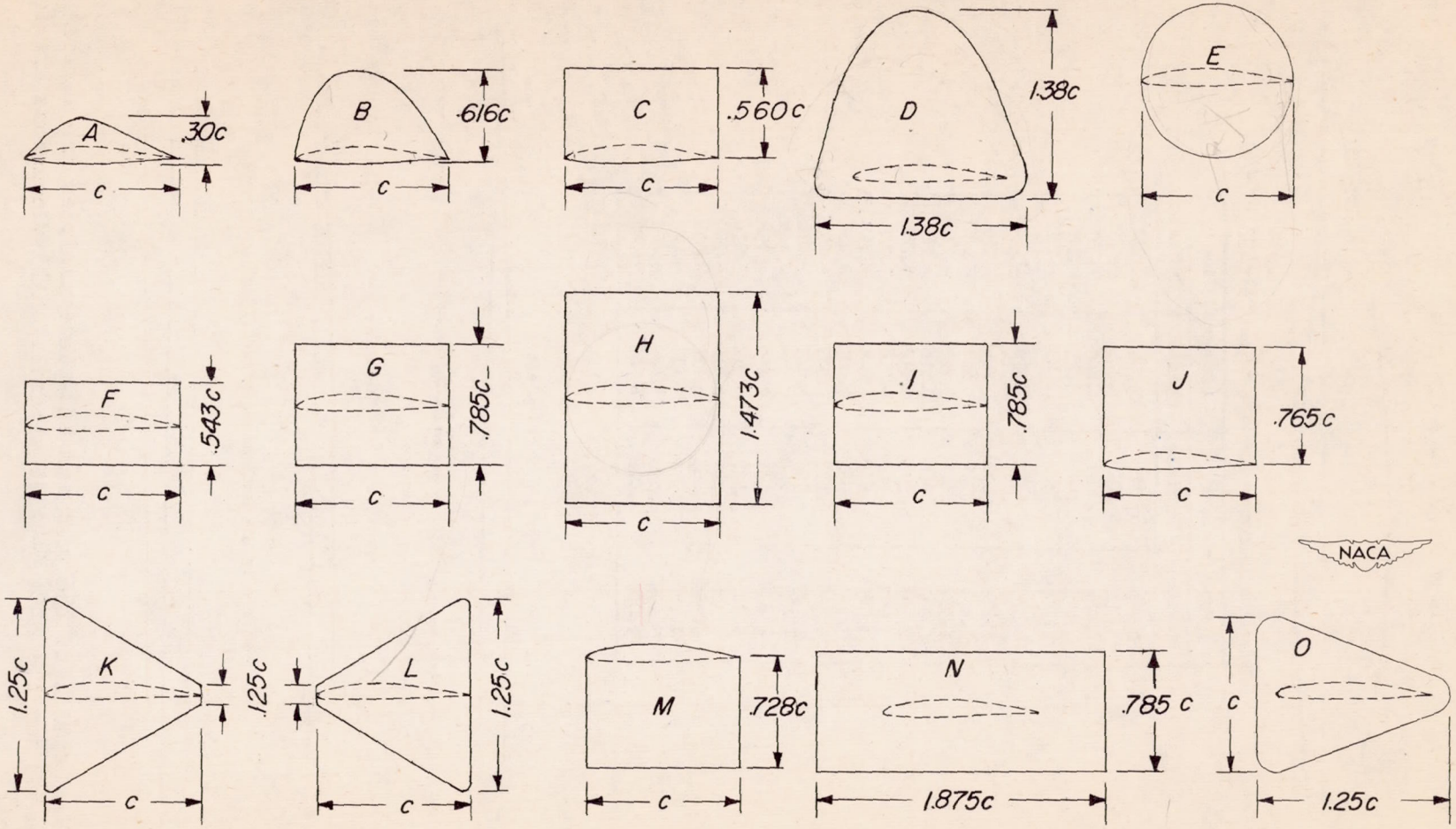

Figure 1.- Plan forms and principal dimensions of the various end plates investigated.

Profile of the NACA 64_1A412 Airfoil

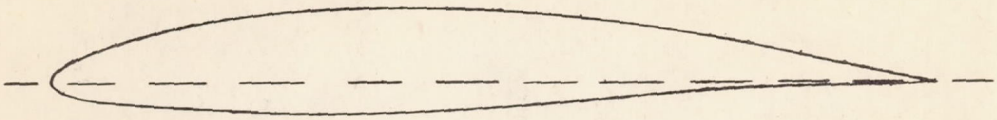

Ordinates in inches for NACA 64_1A412 airfoil (c = 8)

Upper surface		Lower surface	
Station	Ordinate	Station	Ordinate
0.026	0.084	0.054	-0.067
.044	.104	.076	-.079
.082	.135	.118	-.096
.178	.194	.221	-.126
.376	.279	.424	-.164
.575	.346	.625	-.190
.790	.401	.810	-.211
1.176	.490	1.224	-.241
1.578	.559	1.622	-.261
1.981	.611	2.019	-.274
2.384	.648	2.416	-.281
2.788	.673	2.812	-.281
3.192	.684	3.208	-.275
3.595	.679	3.605	-.259
3.999	.661	4.001	-.236
4.398	.632	4.402	-.207
4.795	.592	4.805	-.176
5.192	.544	5.208	-.142
5.590	.487	5.610	-.108
5.988	.422	6.012	-.076
6.386	.349	6.414	-.050
6.786	.265	6.814	-.034
7.190	.179	7.210	-.022
7.595	.090	7.605	-.012
8.000	.002	8.000	-.002

Profile of end plate I

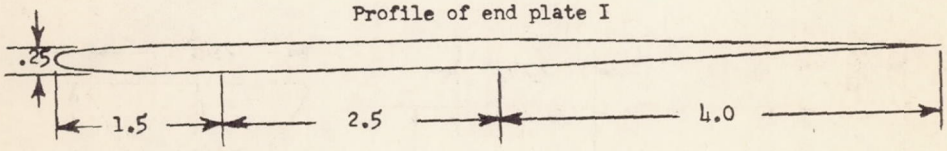

Profile of end plate O

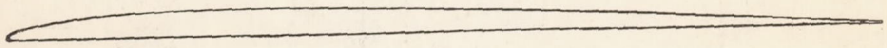

Profile of all end plates except I and O

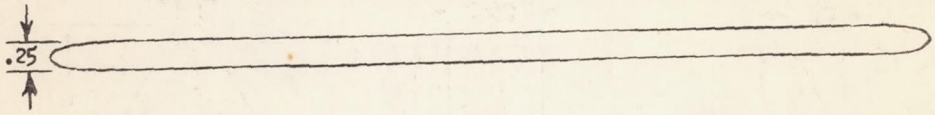

Figure 2.- Details of the wing and end-plate profiles and a table of ordinates for the NACA 64_1A412 airfoil. (All dimensions are in inches.)

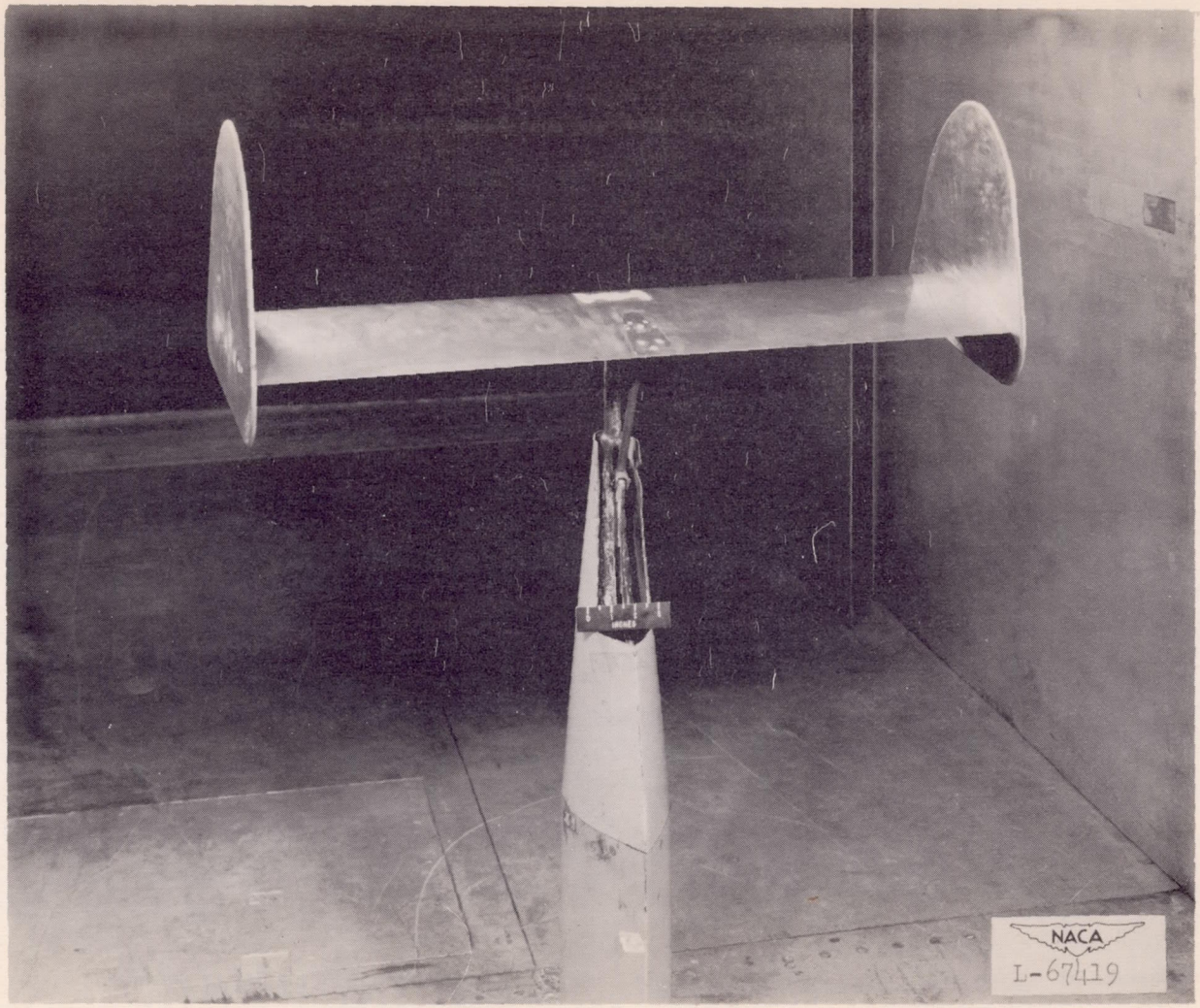

Figure 3.- The wing in combination with end plates D mounted in the 6- by 6-foot test section of the Langley stability tunnel.

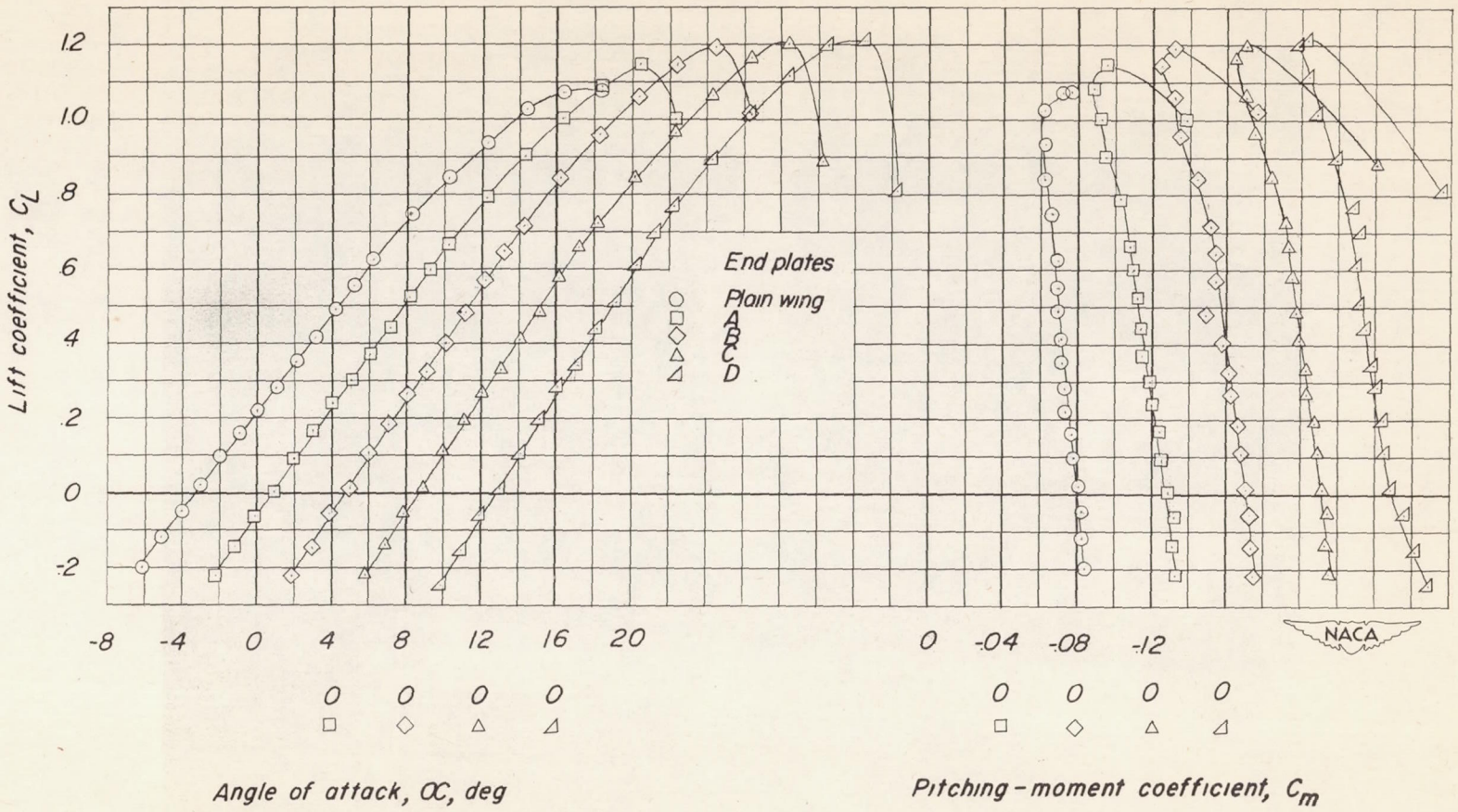

Figure 4.- Lift and pitching-moment characteristics for the wing alone and in combination with the various end plates.

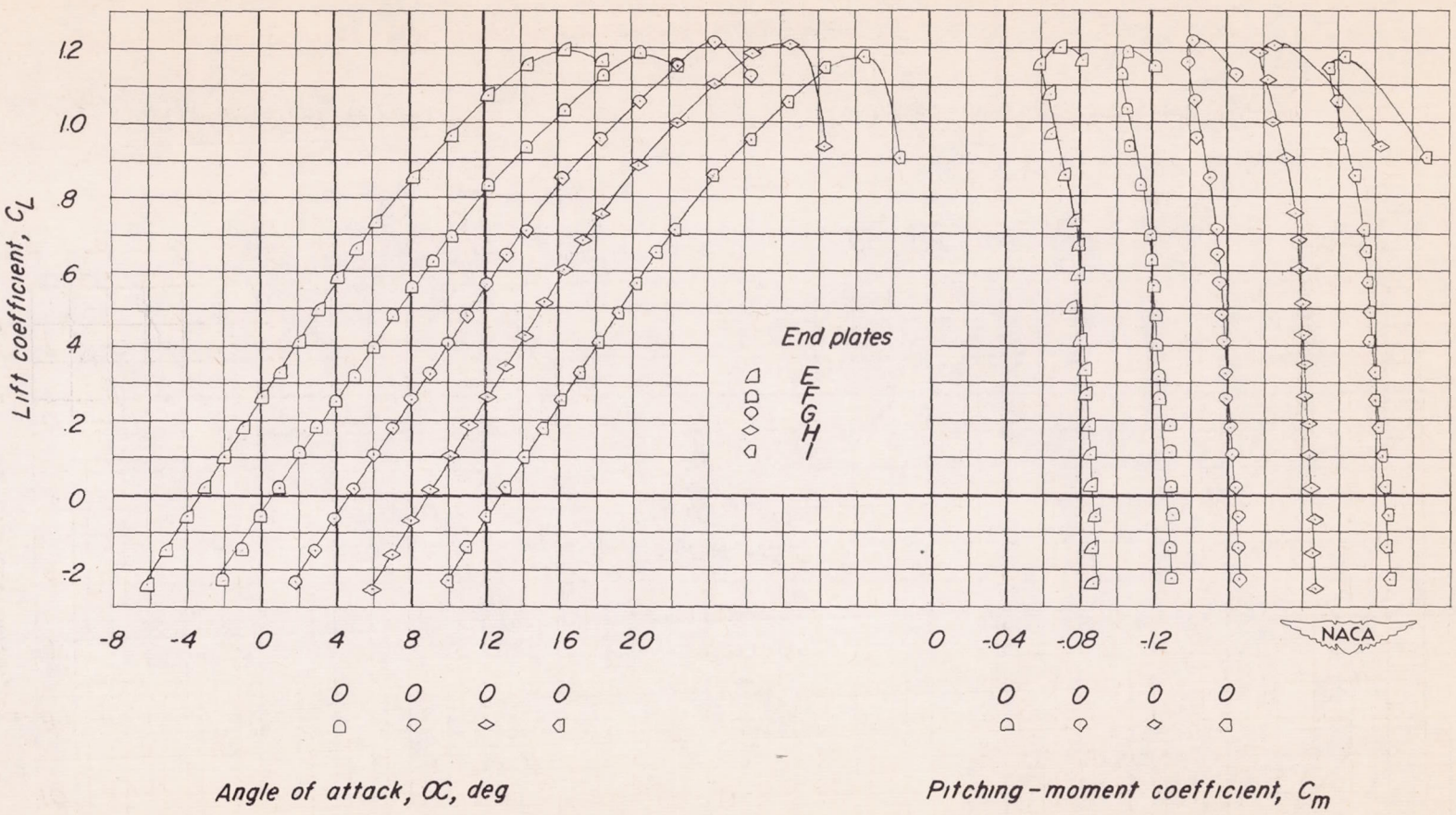

Figure 4.- Continued.

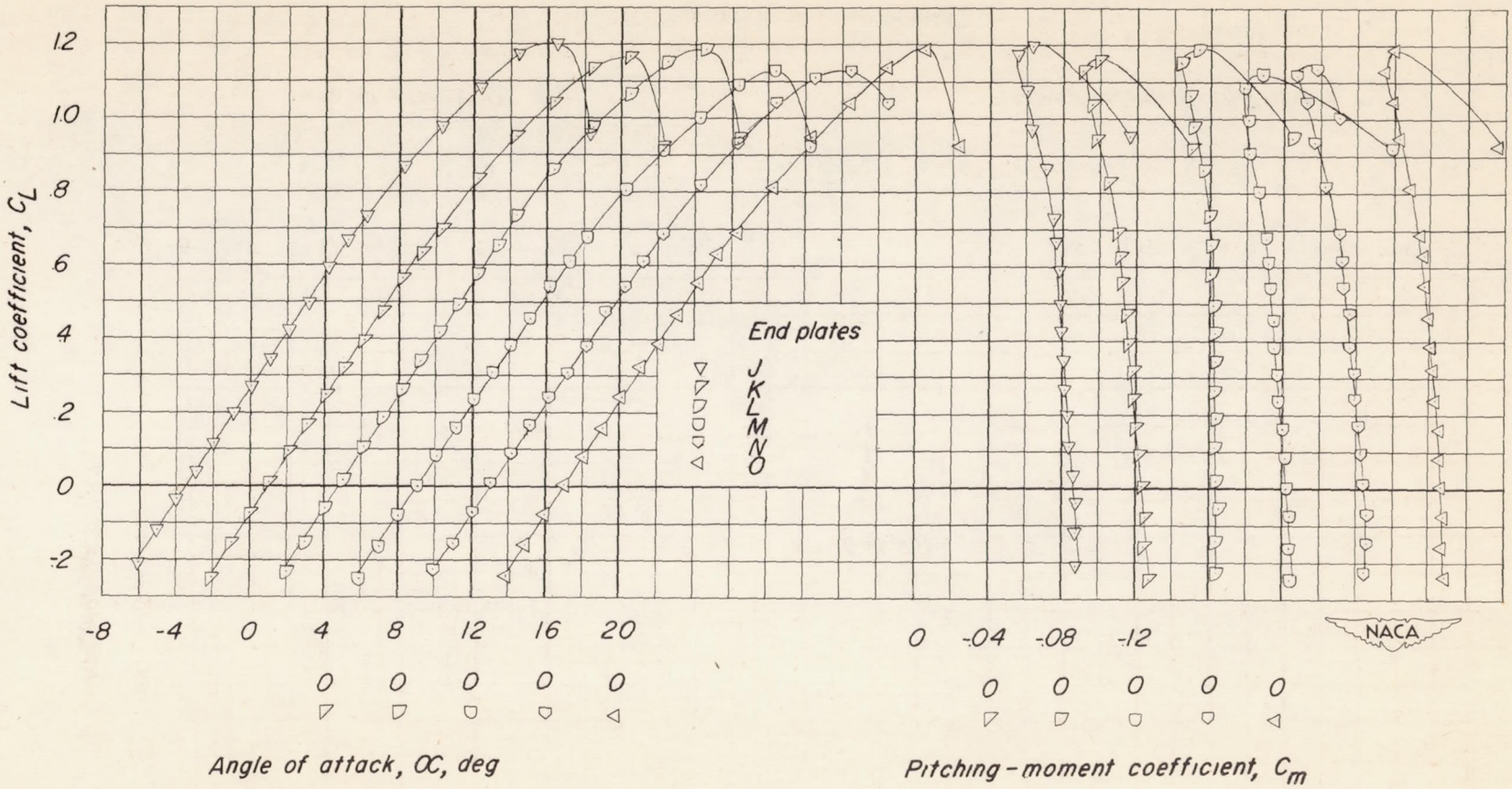

Figure 4.- Concluded.

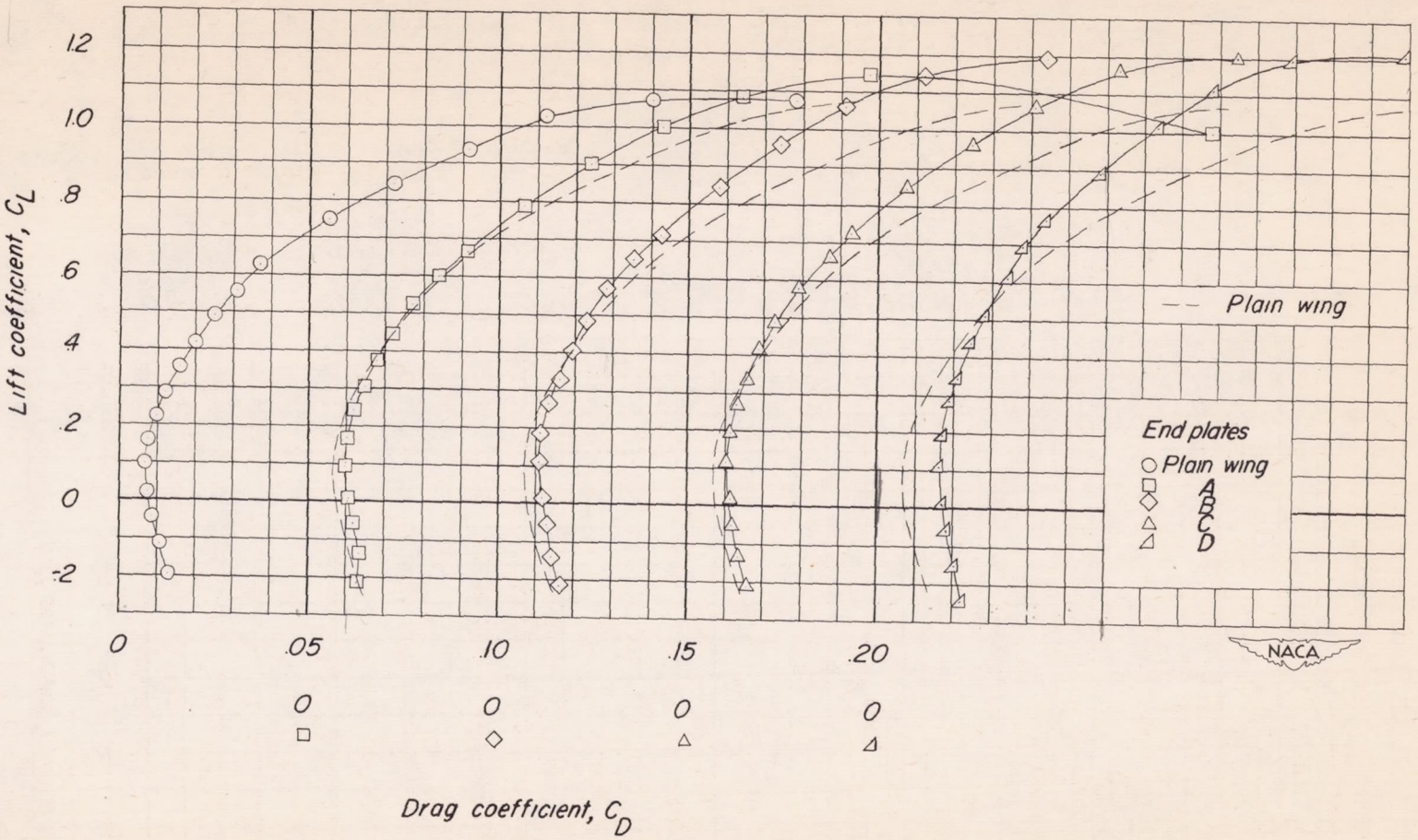

Figure 5.- Comparison of the drag characteristics of the wing alone and in combination with the various end plates.

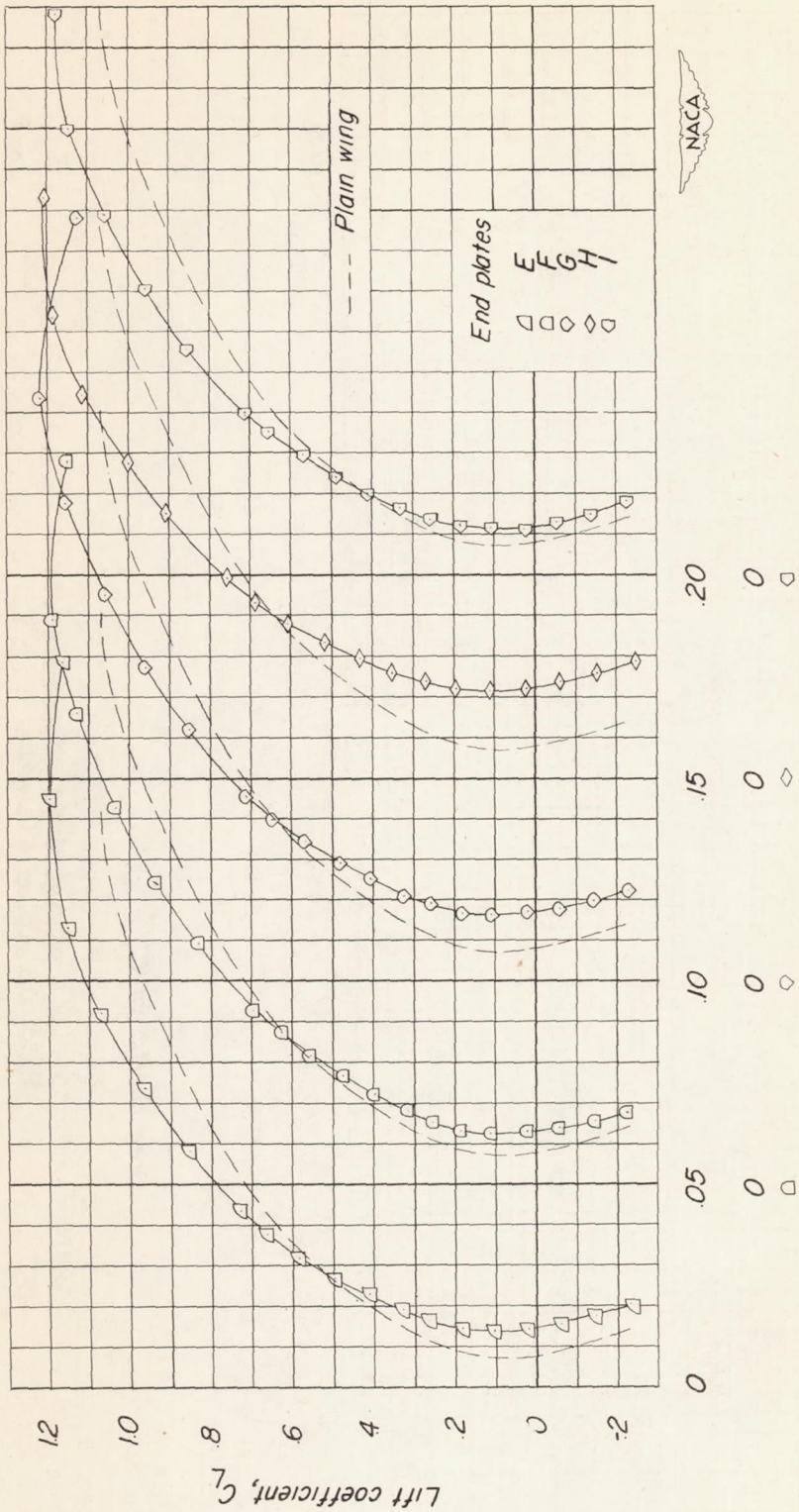

Figure 5.- Continued.

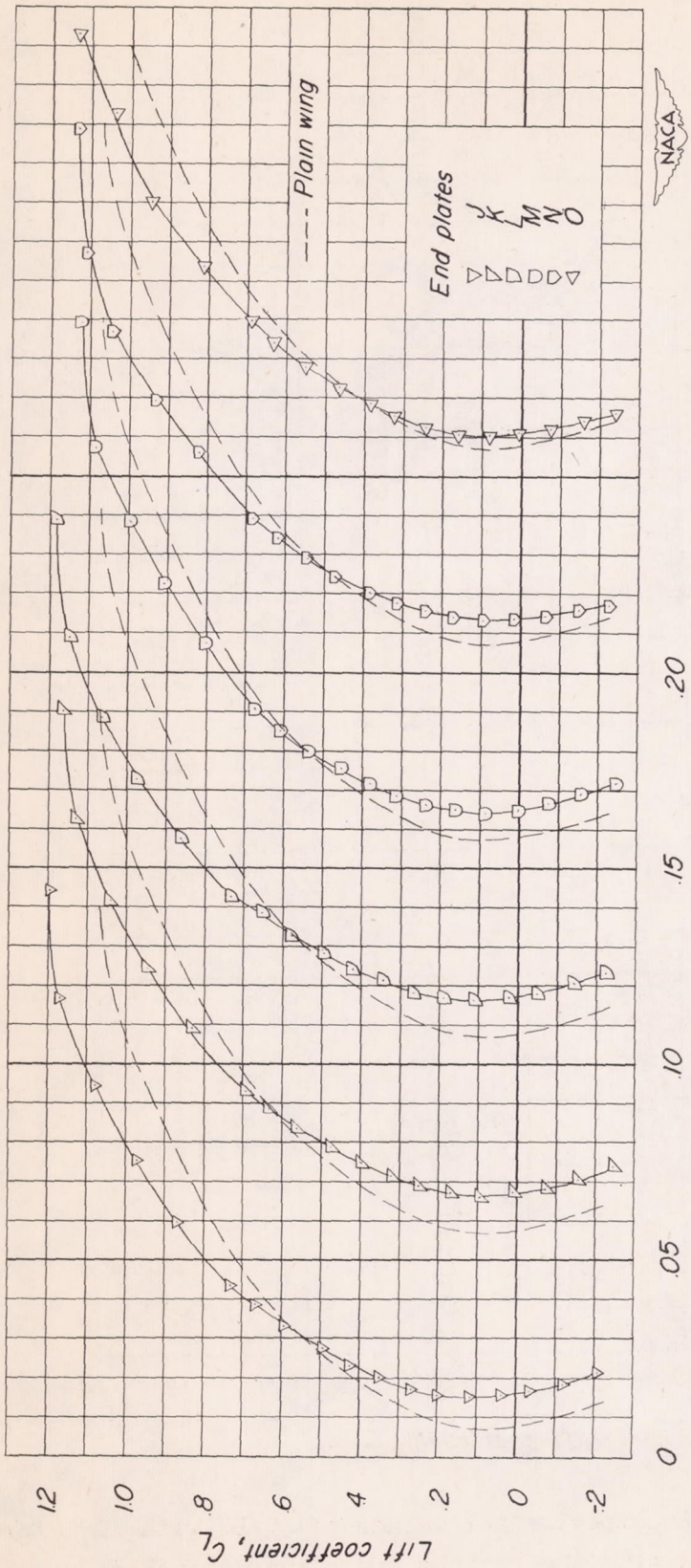

Figure 5.- Concluded.

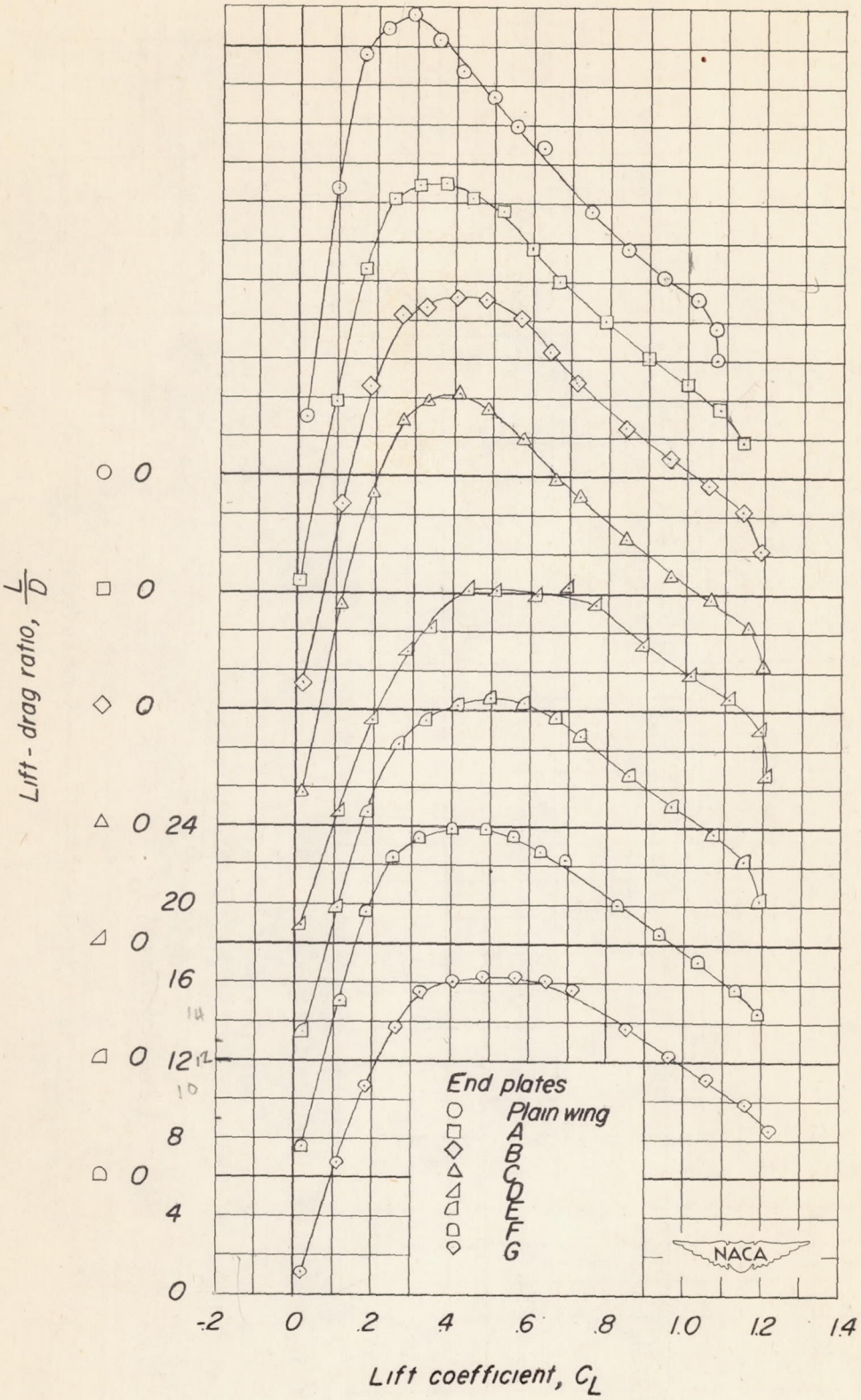

Figure 6.- Variation of the experimental values of L/D with C_L for the wing alone and with the various end plates attached.

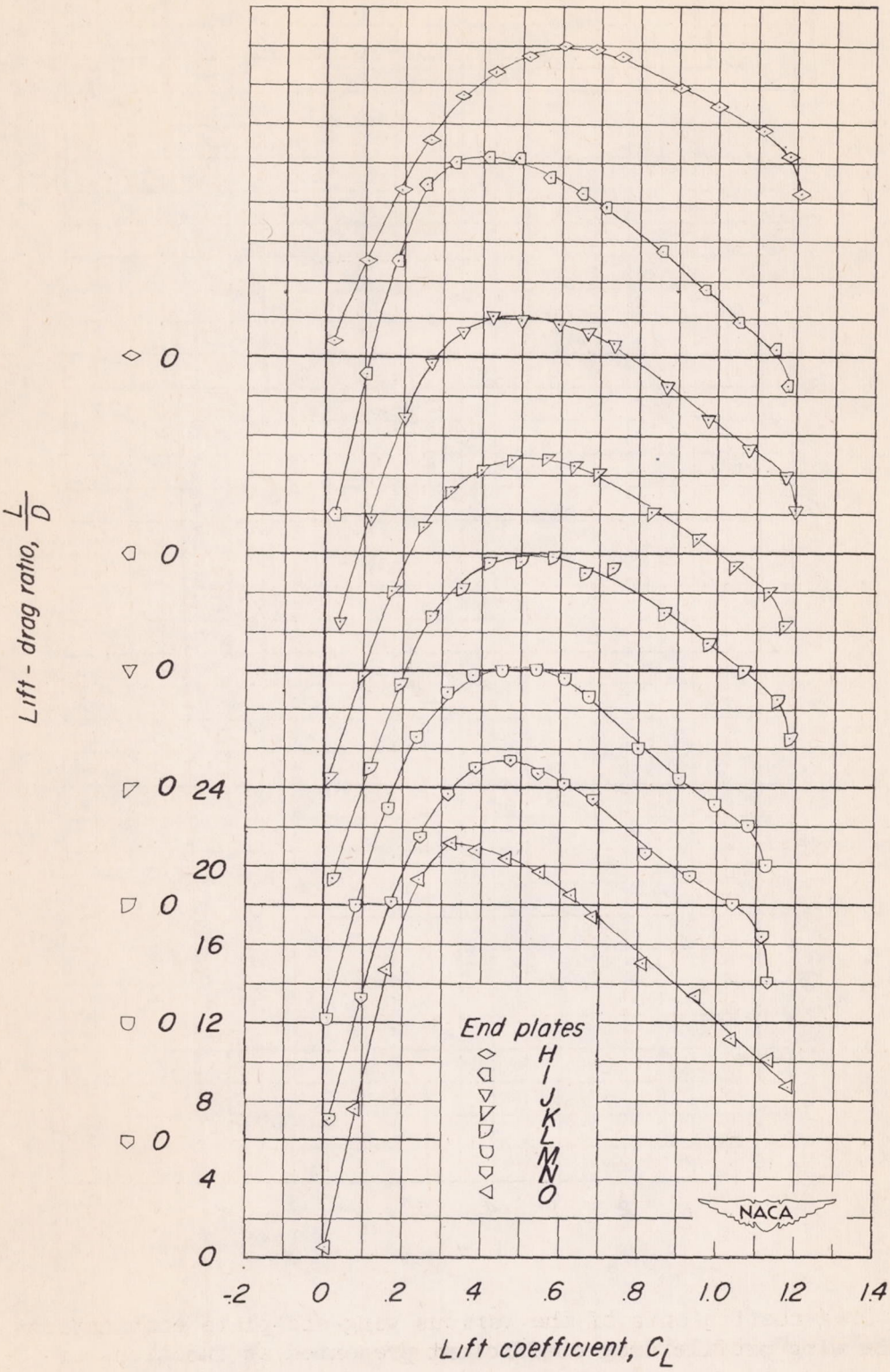

Figure 6.- Concluded.

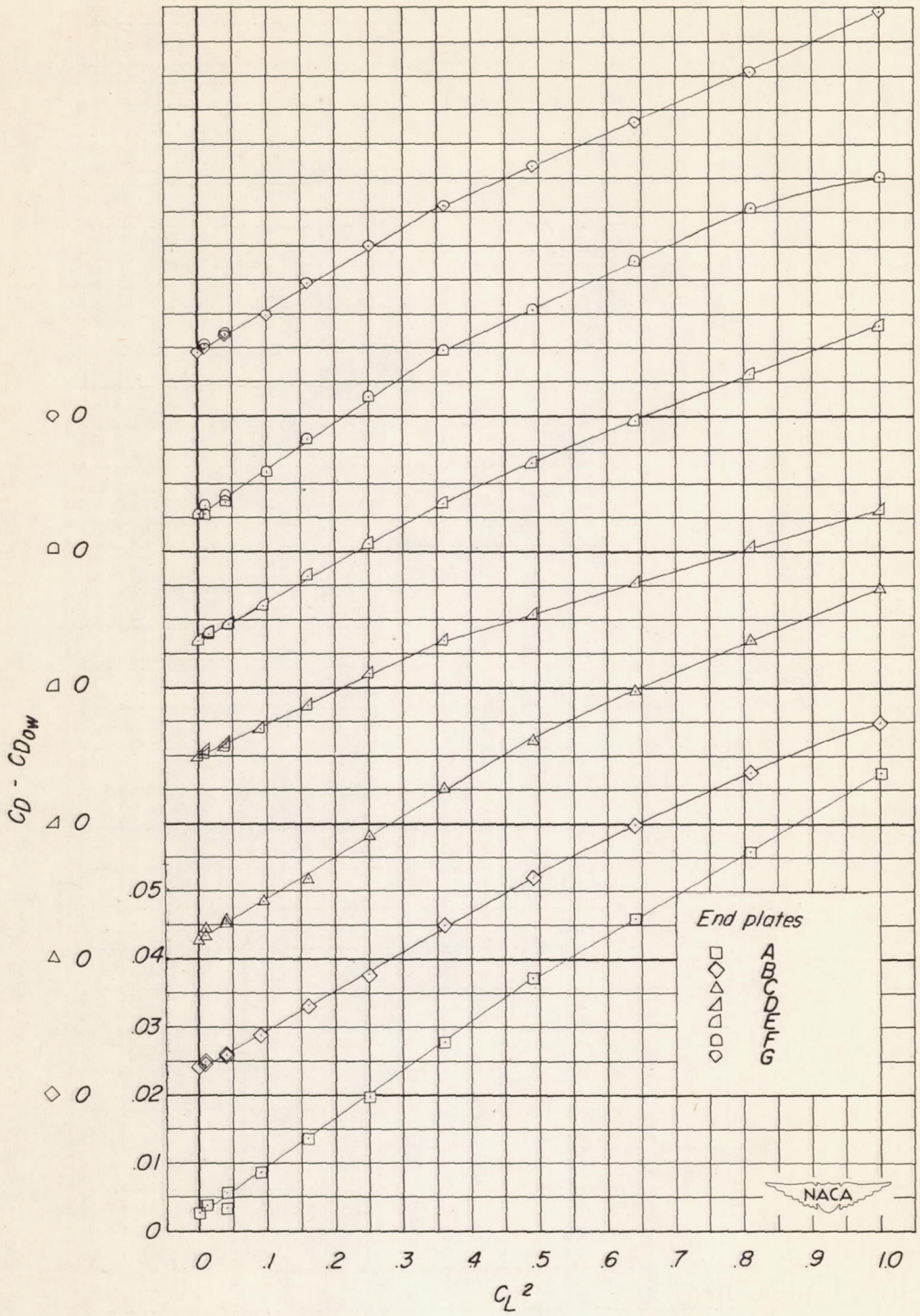

Figure 7.- Drag coefficients of the various wing-end-plate combinations minus the wing profile drag coefficient presented as functions of C_L^2.

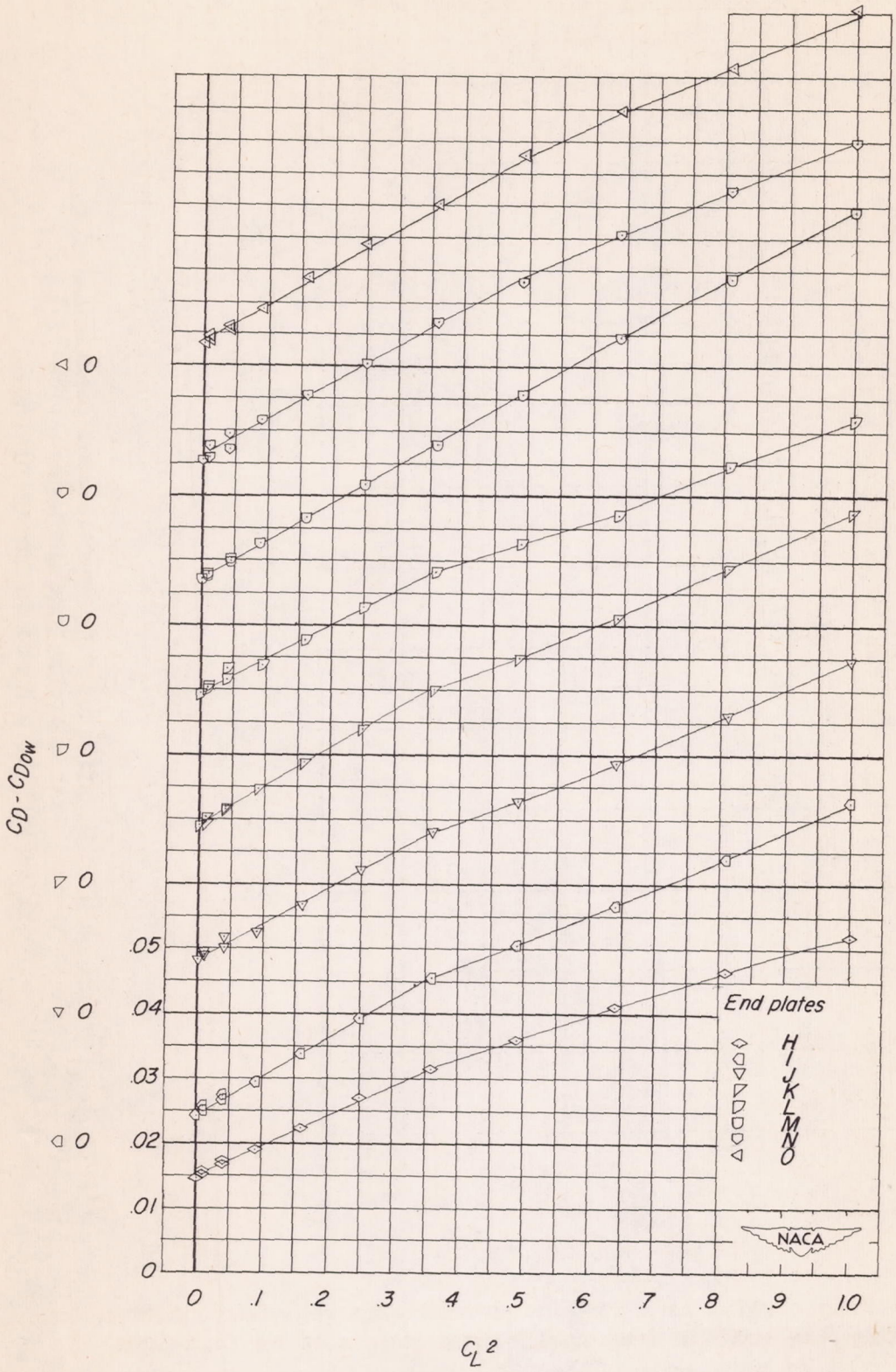

Figure 7.- Concluded.

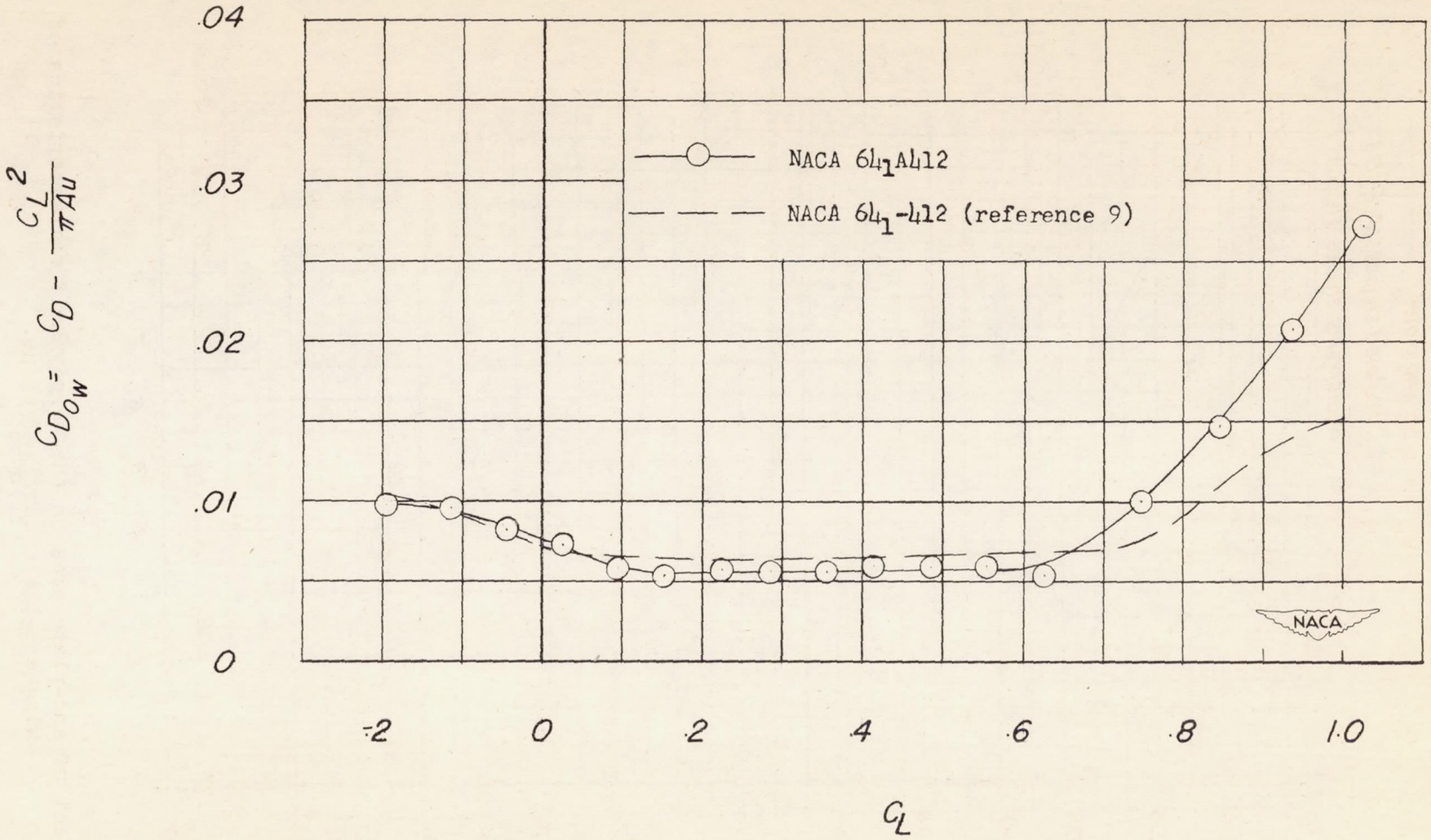

Figure 8.- Comparison of the extracted wing profile drag coefficient for the NACA 64_1A412 airfoil with section drag characteristics of an NACA 64_1-412 airfoil section at a Reynolds number of 1×10^6.

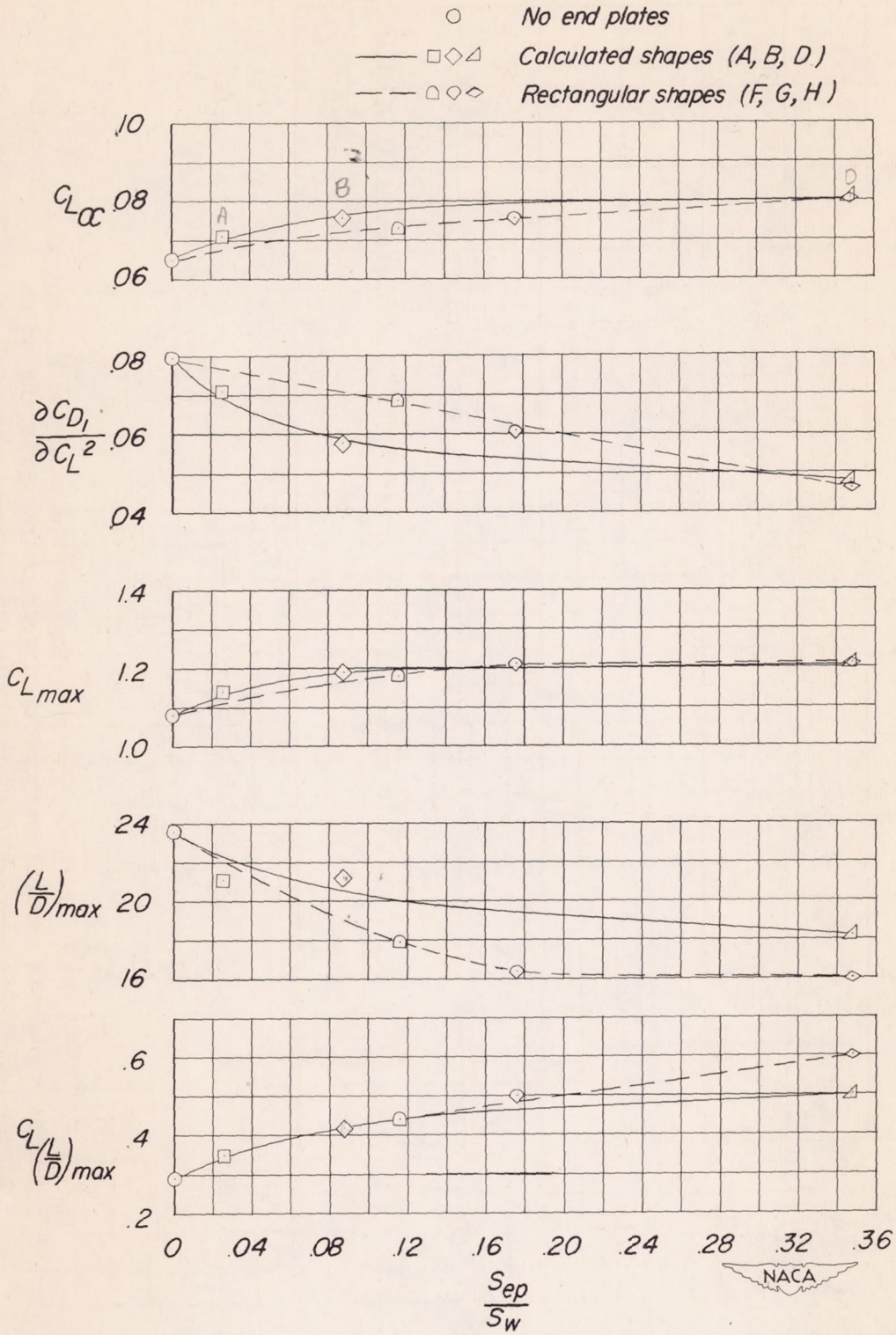

Figure 9.- Effect of end-plate area on the aerodynamic characteristics of wing-end-plate configurations.

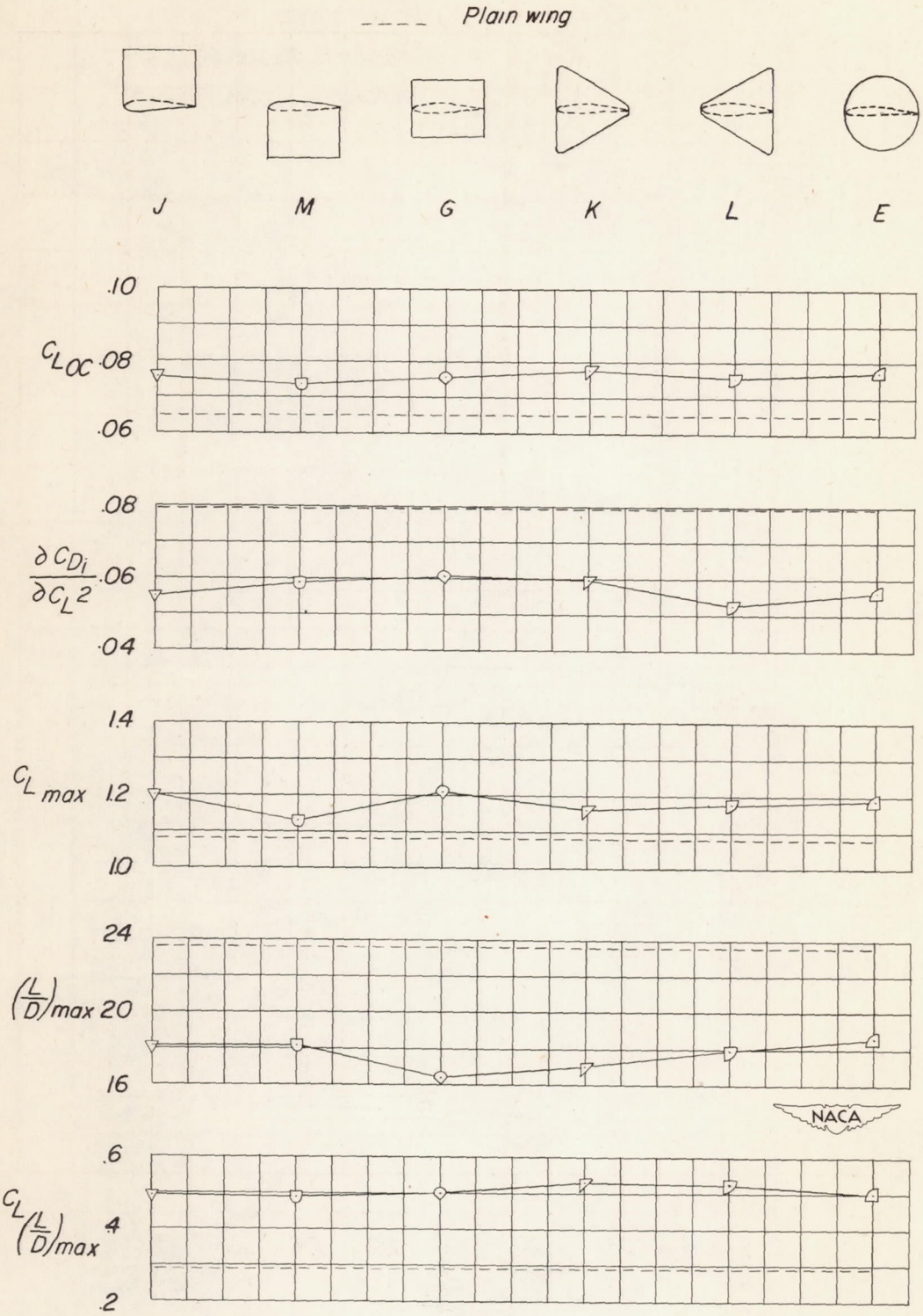

Figure 10.- Effect of end-plate plan form (shape) and location of end-plate area relative to the wing chord line on the aerodynamic characteristics of wing-end-plate configurations.

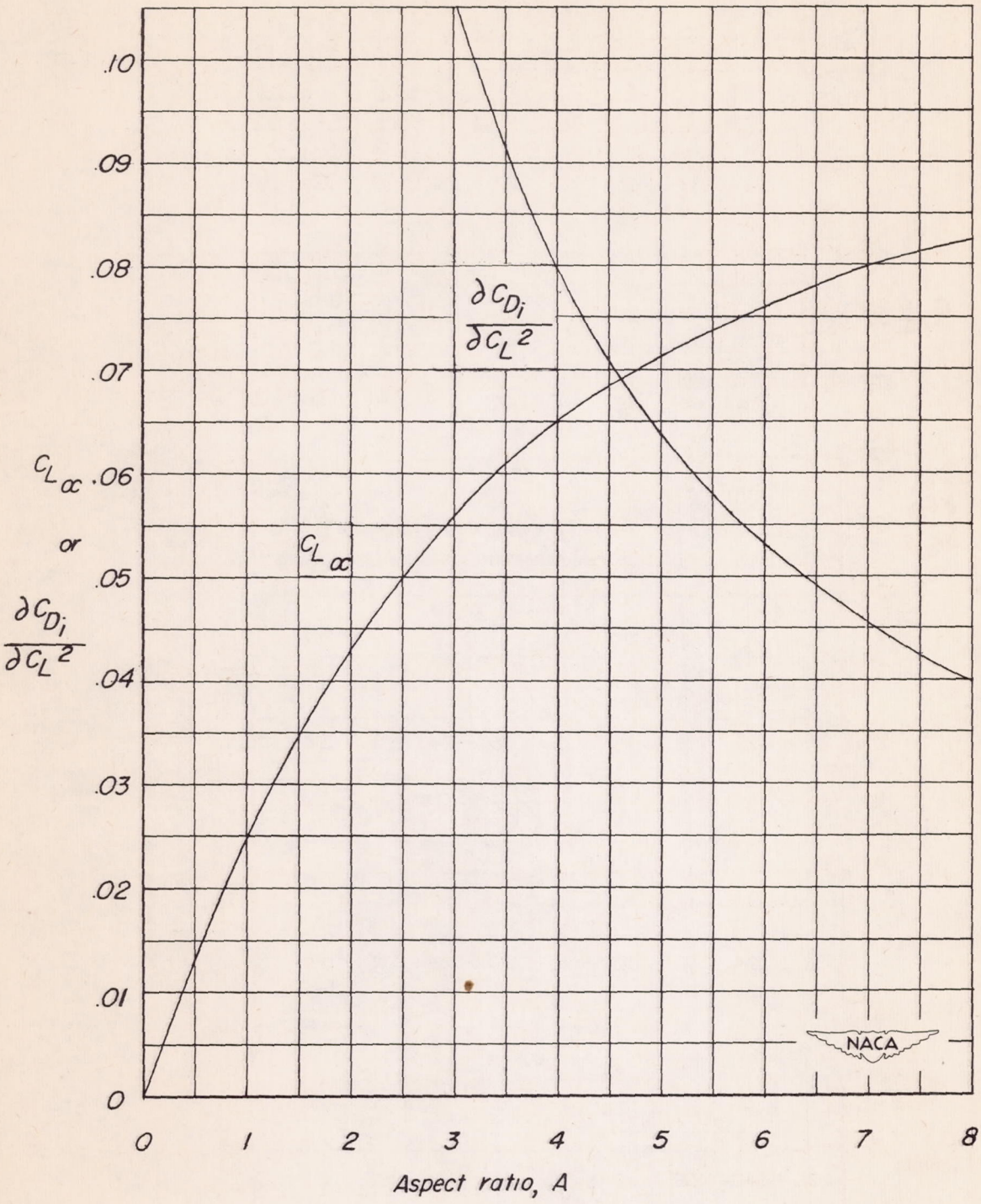

Figure 11.- Chart for the determination of C_{L_α} and $\partial C_{D_i}/\partial C_L^2$ as functions of wing aspect ratio (theoretical variation of C_{L_α} valid only for c_{l_α} of 0.108).

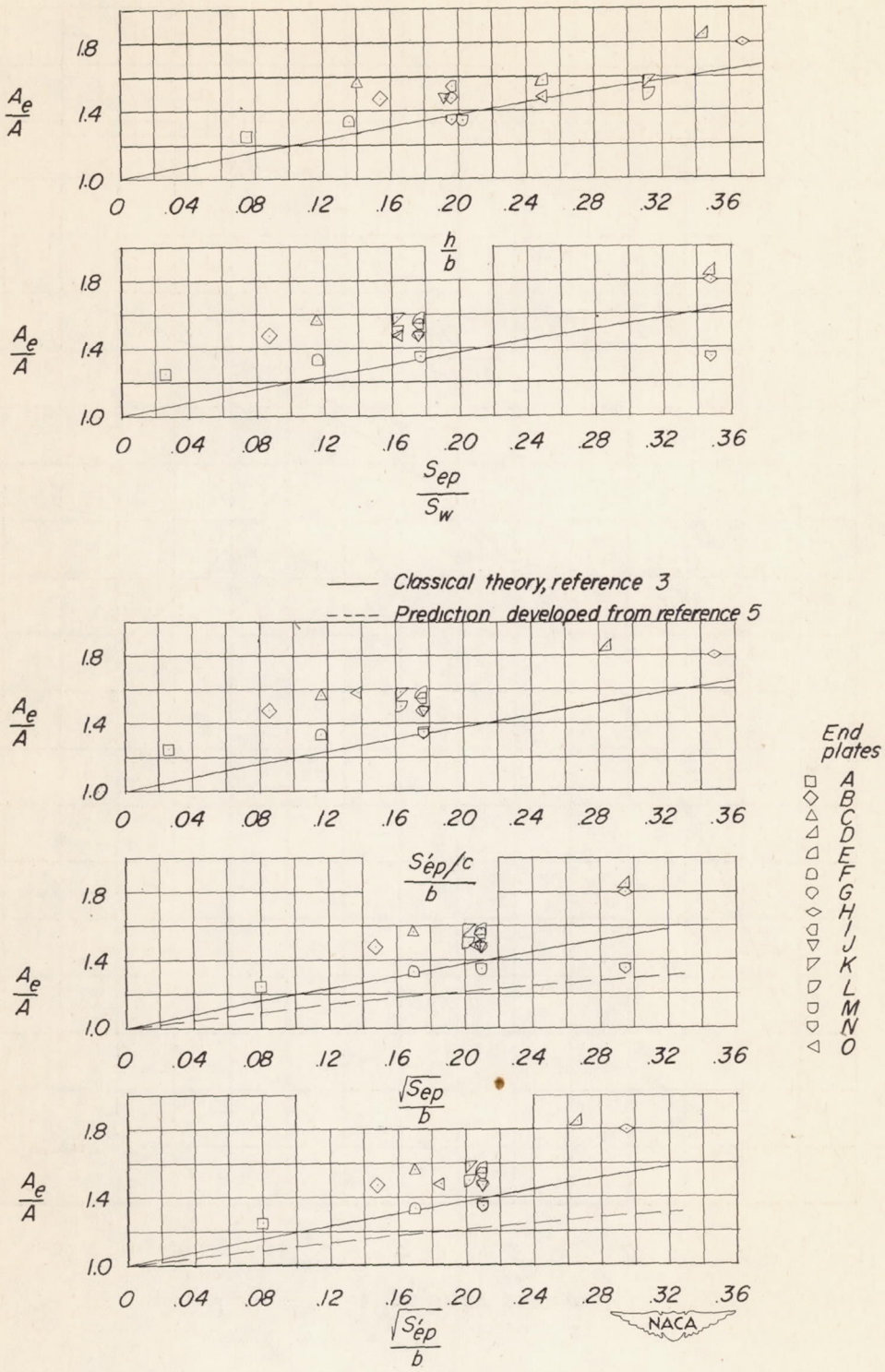

Figure 12.- Comparison of the experimental end-plate effect on C_{L_α} with theoretical and empirical solutions for several different end-plate parameters.

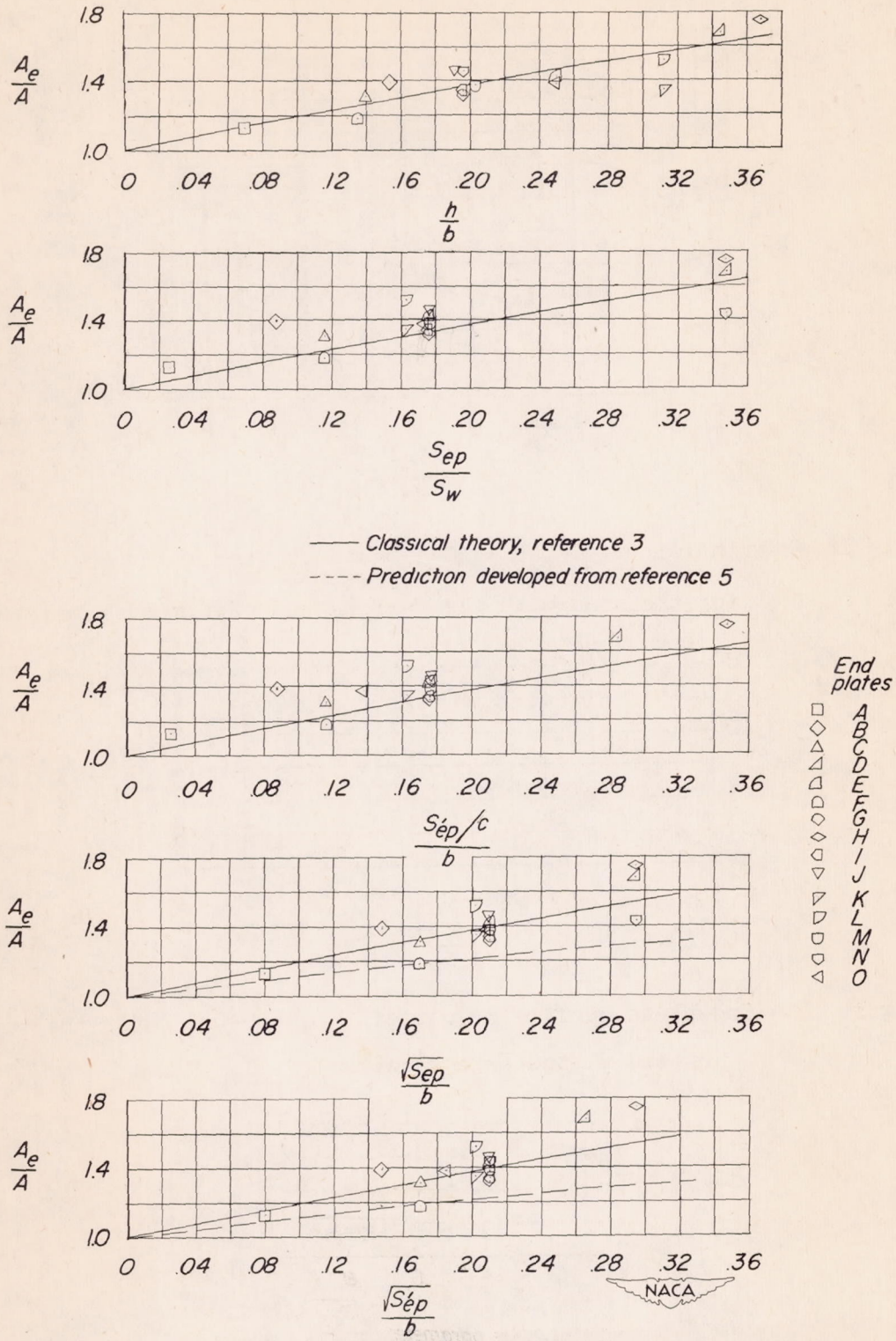

Figure 13.- Comparison of the experimental end-plate effect on $\partial C_{D_i}/\partial C_L^2$ with theoretical and empirical solutions for several end-plate parameters.

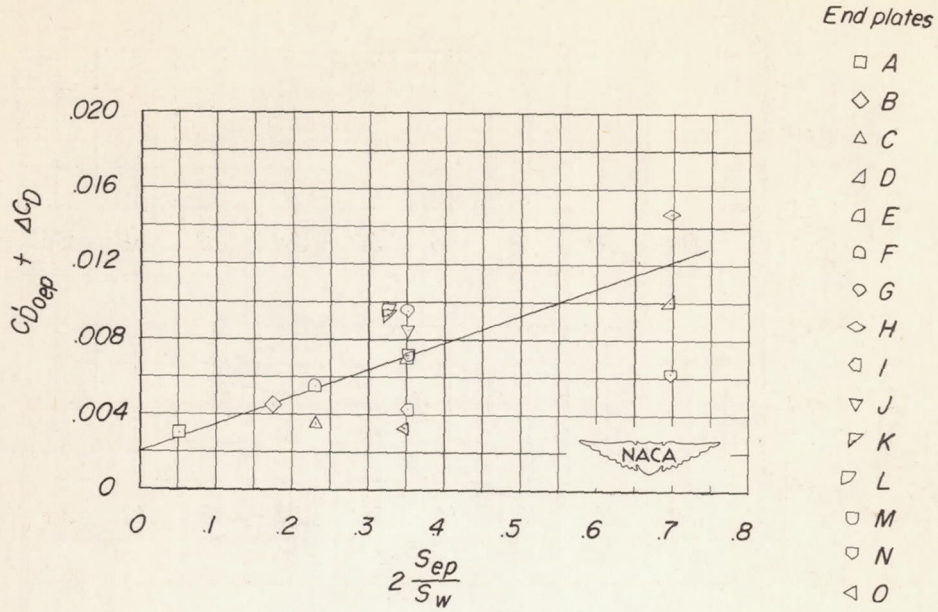

Figure 14.- Variation of $C'_{D_{o_{ep}}} + \Delta C_D$ based on wing area as a function of S_{ep}/S_w for the wing with the various end plates attached. $C_L = 0$.

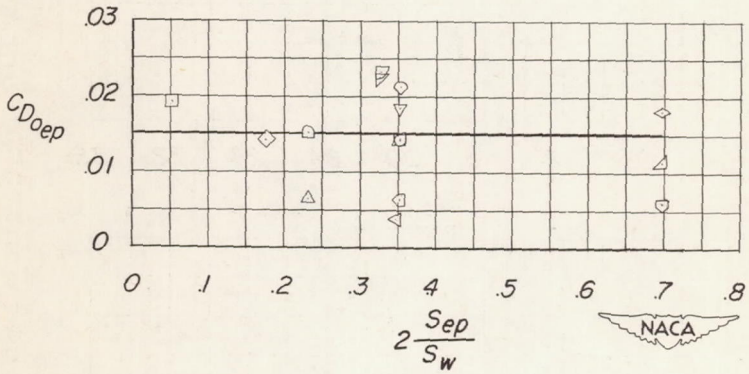

Figure 15.- End-plate profile drag coefficient $C_{D_{o_{ep}}}$ for the various end plates as a function of S_{ep}/S_w.

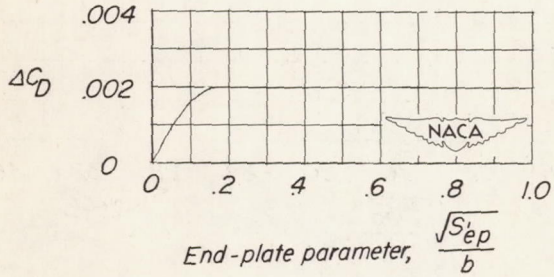

Figure 16.- Assumed variation of ΔC_D as used in the calculations in table I and figures 17 and 18.

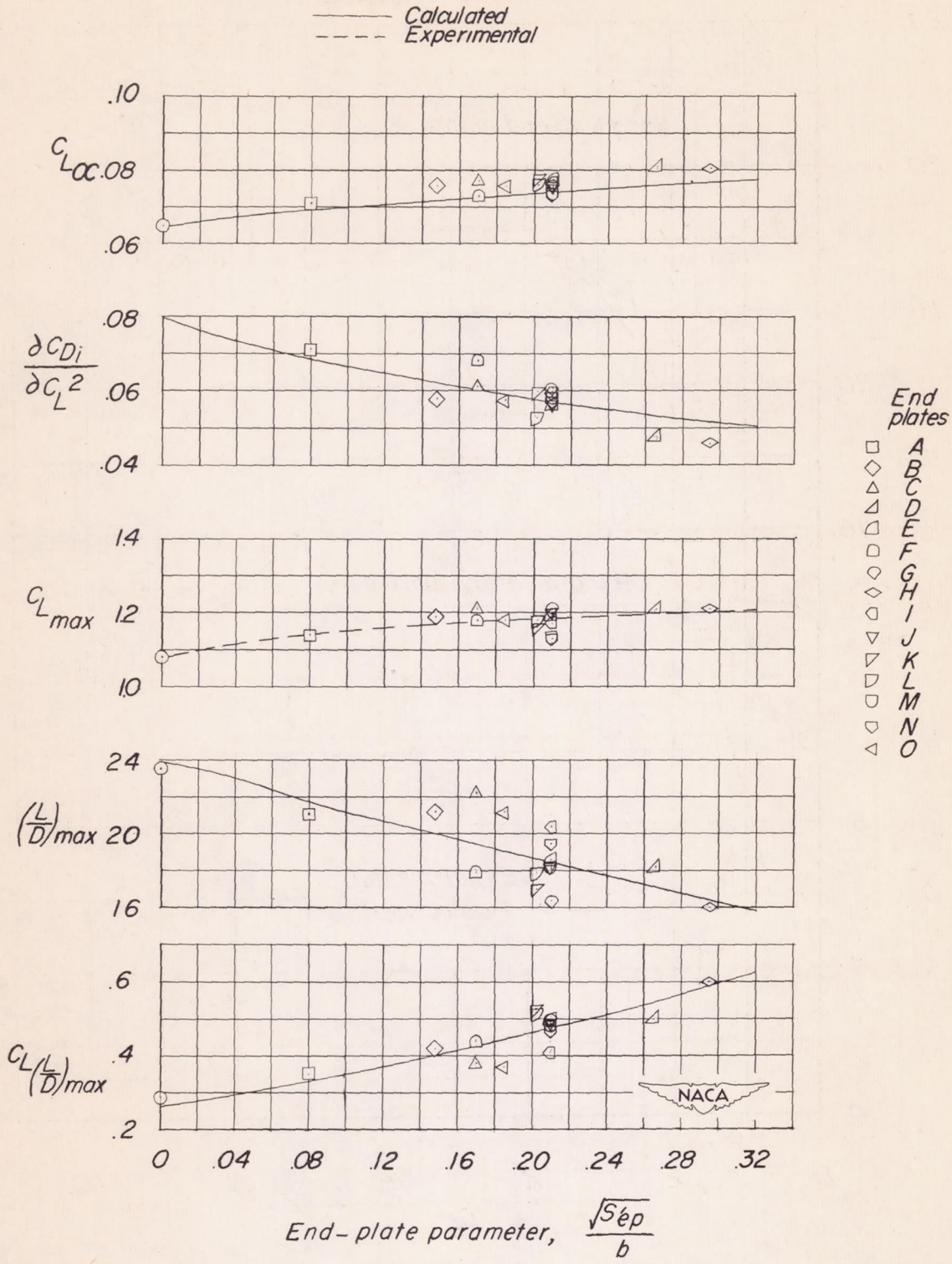

Figure 17.- Comparison of the experimental values with the calculated curves for the various wing-end-plate configurations tested.

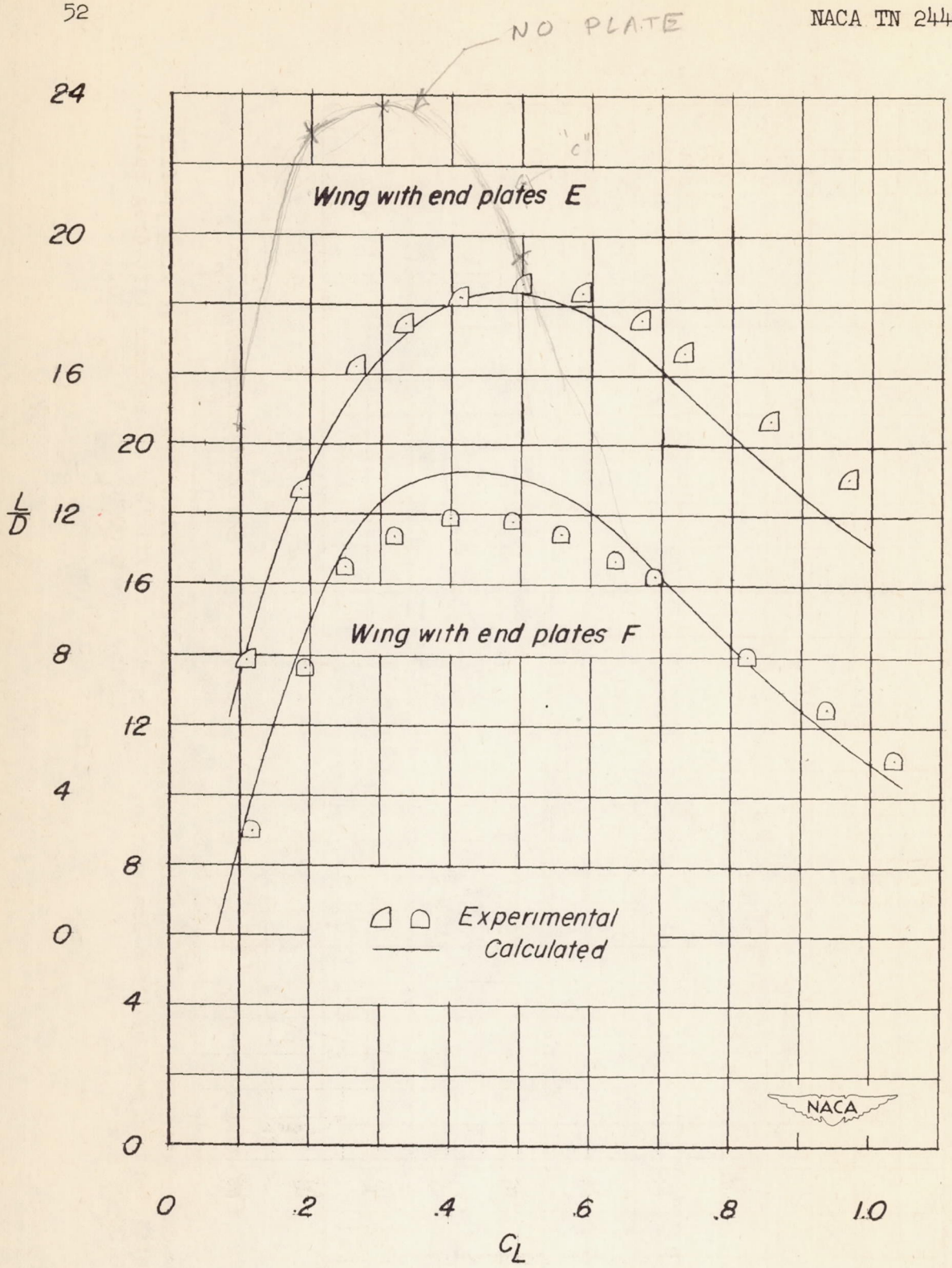

Figure 18.- Comparison of experimental and calculated values of L/D for the wing in combination with end plates E and F.

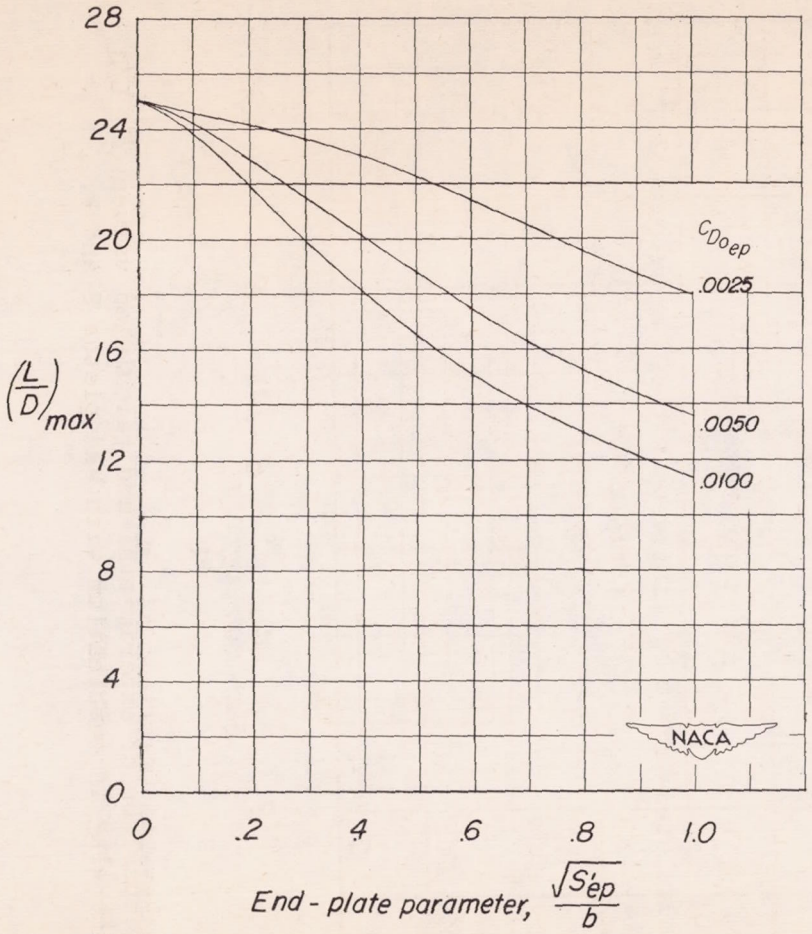

Figure 19.- Calculated effect of end-plate profile drag coefficient on maximum lift-drag ratio. $C_{D_{o_w}} = 0.0050$; $A = 4$; $C_{D_p} = 0$.

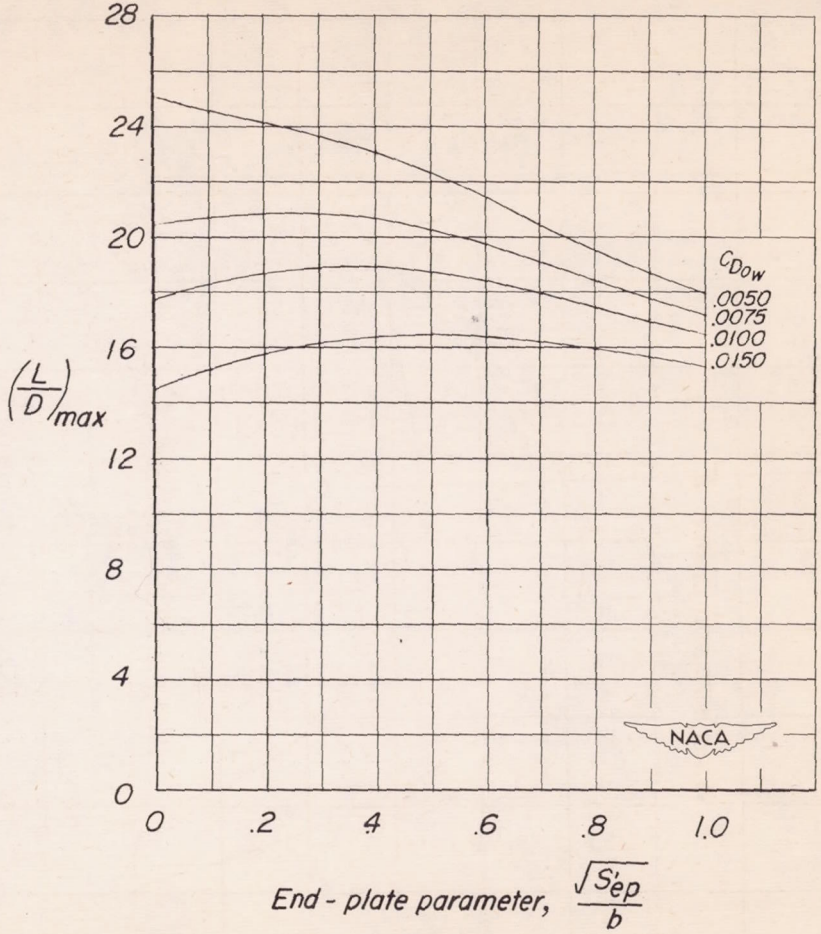

Figure 20.- Calculated effect of wing profile drag coefficient on maximum lift-drag ratio. $C_{D_{o_{ep}}} = 0.0025$; $A = 4$; $C_{D_p} = 0$.

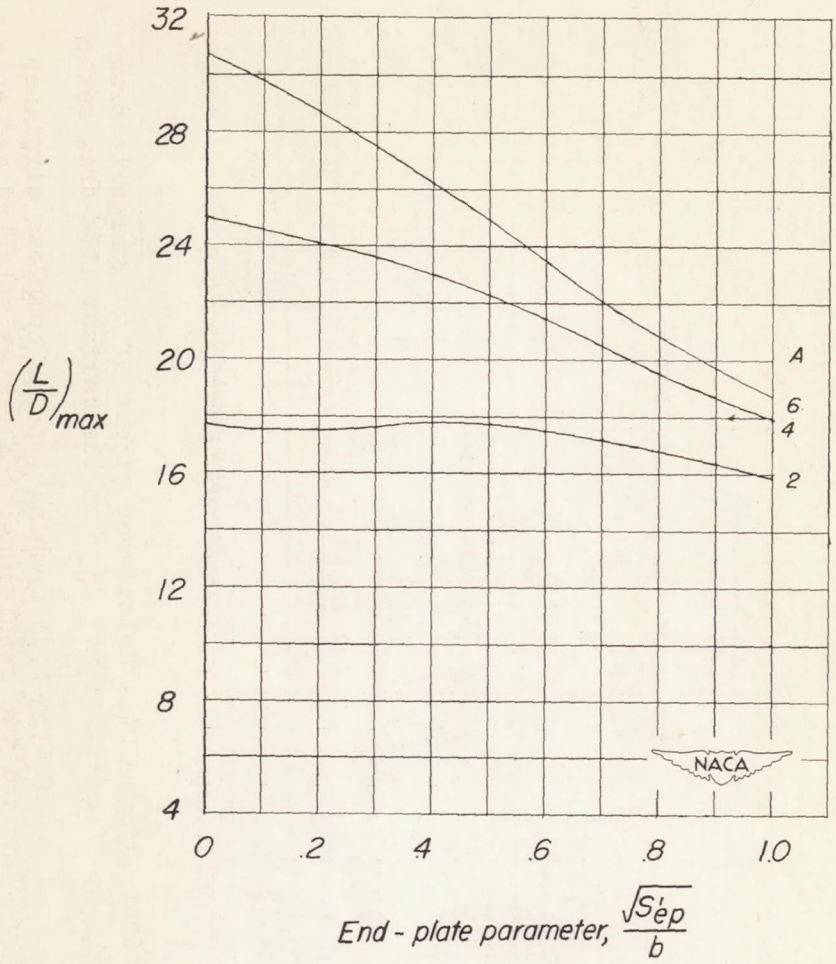

Figure 21.- Calculated effect of wing aspect ratio on maximum lift-drag ratio. $C_{D_{o_w}} = 0.0050$; $C_{D_{o_{ep}}} = 0.0025$; $C_{D_p} = 0$.

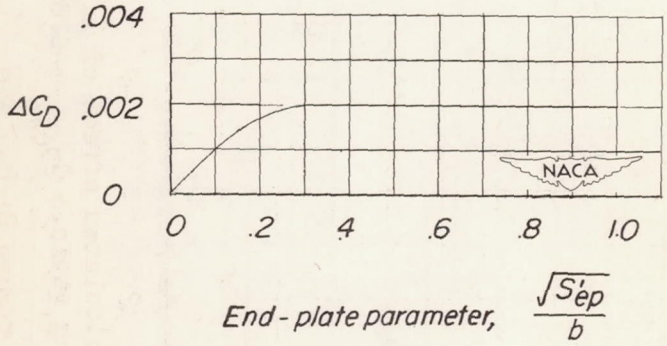

Figure 22.- Assumed variation of ΔC_D with $\sqrt{S'_{ep}}/b$ used in the calculations for figures 19, 20, 21, 23, and 24.

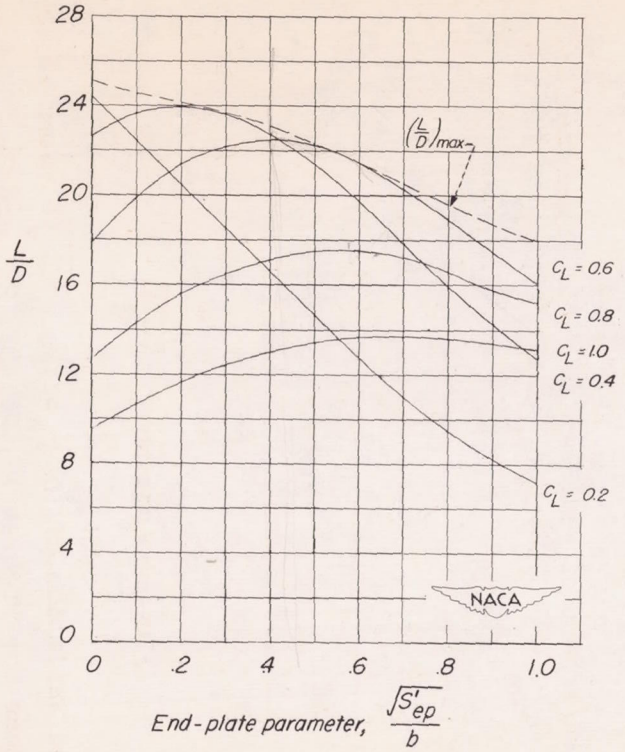

Figure 23.- Calculated effect of lift coefficient on lift-drag ratio. $C_{D_{o_{ep}}} = 0.0025$; $A = 4$; $C_{D_{o_w}}$ from figure 8; $C_{D_p} = 0$.

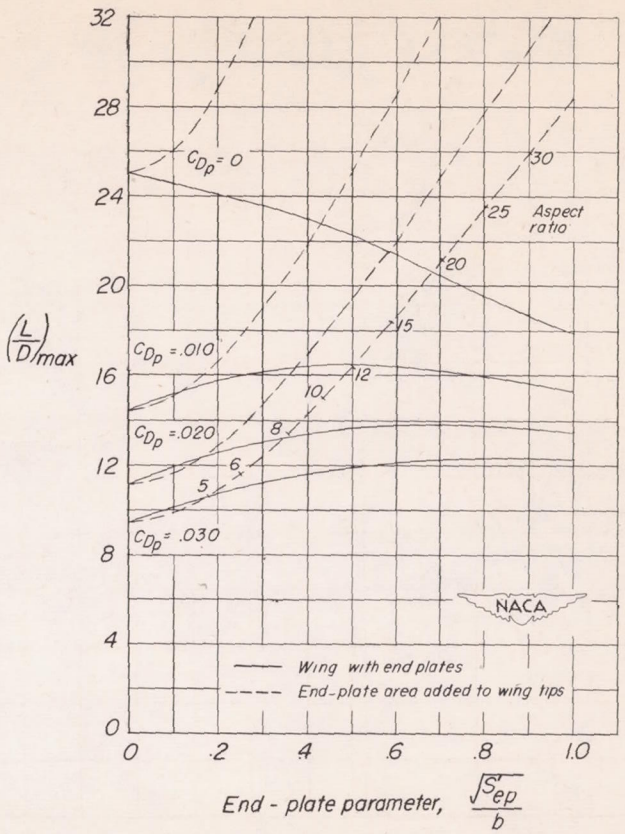

Figure 24.- Calculated effect of the parasite drag coefficient C_{D_p} on the maximum lift-drag ratio of wing-body combinations or complete airplanes for two conditions; end plates attached and end-plate area added to the wing tips. $C_{D_{o_{ep}}} = 0.0025$; $A = 4$; $C_{D_{o_w}} = 0.005$.

NACA-Langley - 8-21-51 - 1000